

# Variations in flow and transport in thick desert vadose zones in response to paleoclimatic forcing (0–90 kyr): Field measurements, modeling, and uncertainties

Bridget R. Scanlon, Kelley Keese, and Robert C. Reedy

Bureau of Economic Geology, Jackson School of Geosciences, University of Texas at Austin, Austin, Texas, USA

Jirka Simunek

George E. Brown, Jr., Salinity Laboratory, Riverside, California, USA

Brian J. Andraski

U.S. Geological Survey, Carson City, Nevada, USA

Received 23 July 2002; revised 29 January 2003; accepted 31 March 2003; published 10 July 2003.

[1] An understanding of unsaturated flow and potential recharge in interdrainage semiarid and arid regions is critical for quantification of water resources and contaminant transport. We evaluated system response to paleoclimatic forcing using water potential and Cl profiles and modeling of nonisothermal liquid and vapor flow and Cl transport at semiarid (High Plains, Texas) and arid (Chihuahuan Desert, Texas; Amargosa Desert, Nevada) sites. Infiltration in response to current climatic forcing is restricted to the shallow (~0.3–3 m) subsurface. Subsurface Cl accumulations correspond to time periods of 9–90 kyr. Bulge-shaped Cl profiles generally represent accumulation during the Holocene (9–16 kyr). Lower Cl concentrations at depth reflect higher water fluxes (0.04–8.4 mm/yr) during the Pleistocene and earlier times. Low water potentials and upward gradients indicate current drying conditions. Nonisothermal liquid and vapor flow simulations indicate that upward flow for at least 1–2 kyr in the High Plains and for 12–16 kyr at the Chihuahuan and Amargosa desert sites is required to reproduce measured upward water potential gradients and that recharge is negligible (<0.1 mm/yr) in these interdrainage areas. *INDEX TERMS:* 1809 Hydrology: Desertification; 1815 Hydrology: Erosion and sedimentation; 1833 Hydrology: Hydroclimatology; *KEYWORDS:* paleoclimate, chloride mass balance, unsaturated zone, unsaturated flow modeling

**Citation:** Scanlon, B. R., K. Keese, R. C. Reedy, J. Simunek, and B. J. Andraski, Variations in flow and transport in thick desert vadose zones in response to paleoclimatic forcing (0–90 kyr): Field measurements, modeling, and uncertainties, *Water Resour. Res.*, 39(7), 1179, doi:10.1029/2002WR001604, 2003.

## 1. Introduction

[2] Quantification of water resources is a critical issue for many desert regions, particularly in the southwestern United States, where water demand is increasing with increasing populations. Interdrainage semiarid and arid regions represent significant portions of watersheds; therefore evaluating whether there is diffuse recharge or no recharge in these regions is important for water resources. Waste disposal is also an important issue for semiarid and arid regions because they are considered much more suitable than humid regions for this purpose [Reith and Thompson, 1992]. Determining whether water is moving up or down is critical for recharge and contaminant transport. This basic question is difficult to resolve in many interdrainage, semiarid and arid regions because water fluxes are extremely low (~mm/yr [Phillips, 1994]). The low fluxes result in thick vadose zones providing an archive of system response to paleoclimatic fluctua-

tions [Tyler *et al.*, 1996]. Understanding the current system at different depths requires evaluation of system response to past climate fluctuations, which, in turn, requires an understanding of the following issues: (1) How deep does water penetrate under current climatic fluctuations? (2) What is the spatial and temporal variability in estimated water fluxes and ages from Cl profiles? (3) What timescales are represented by upward water potential gradients? (4) How important is vapor flow?

[3] The purpose of this study was to evaluate variations in flow and transport in thick desert vadose zones in response to paleoclimatic forcing using field measurements and modeling analysis. Water potential and Cl profiles from several sites (High Plains and Chihuahuan Desert, Texas, and Amargosa Desert, Nevada) were used in the analysis. This study addresses many of the above issues, including penetration depths of wetting fronts in response to seasonal and annual climatic forcing using long-term (5–12 yr) water potential monitoring records, variability in water fluxes and ages calculated from Cl profiles at the different sites, and timescales of upward flow related to upward water potential

gradients and relative importance of liquid and vapor flow using numerical modeling. Unique aspects of this study include the range of current climatic conditions (mean annual precipitation 108–500 mm/yr) and of sediment types (clay loam to sand) at the different sites, length of water potential monitoring records (5–12 yr), and collocation of water potential and Cl profiles. Numerical modeling of nonisothermal liquid and vapor flow plays a critical role in evaluating system response to paleoclimatic fluctuations and assessing important processes (upward versus downward flux, liquid and vapor flux) and controls (e.g., climate, vegetation, and sediment texture) on subsurface flow and transport. Uncertainties in all aspects of the study, including measurements, monitoring, and modeling, are evaluated to identify gaps in our knowledge and areas of future research.

### 1.1. Background

[4] Direction of water movement can be determined using potential energy gradients in isothermal systems because water moves from regions of high energy to regions of low energy [Jury *et al.*, 1991]. Gravitational potential is equal to the elevation above a datum, such as the water table. Matric potential describes the forces related to the soil matrix and is dominated by capillary forces under wet conditions and adsorptive forces under dry conditions. Osmotic potential results from the addition of solutes to the pore water. Water potential includes matric and osmotic potential and can be measured by thermocouple psychrometers. Typical water potentials in many semiarid and arid settings are lowest near the surface ( $\sim -400$  to  $-1000$  m) and increase exponentially with depth, indicating an upward driving force for water movement [Scanlon, 1994; Andraski, 1997; Izbicki *et al.*, 2000; Walvoord *et al.*, 2002]. Relating water potential profiles to paleoclimatic forcing requires an understanding of how water potential variations are related to seasonal and annual climatic fluctuations.

[5] Chloride concentrations in unsaturated zone pore water have been measured at many of the sites where water potentials have been measured [Andraski and Prudic, 1997; Scanlon *et al.*, 1999; Izbicki *et al.*, 2000; Walvoord *et al.*, 2002]. The Cl mass balance (CMB) approach was used to quantify water fluxes on millennial timescales at these sites. Water flux is calculated by dividing the Cl input (precipitation  $\times$  Cl concentration in precipitation and dry fallout) by the Cl concentration in unsaturated zone pore water. The age represented by Cl is calculated by dividing the cumulative mass of Cl from the surface to the depth of interest by the Cl input. One of the primary assumptions of the CMB approach is that water is moving downward through the unsaturated zone. Bulge-shaped Cl profiles at these sites are characterized by increasing concentrations to a maximum near the base of the root zone and decreasing to much lower concentrations at depth. These profiles are typical of desert regions in the southwestern United States [Phillips, 1994]. The low Cl concentrations beneath the bulges have been attributed to higher water fluxes during pluvial conditions (mesic vegetation) in the Pleistocene ( $\geq 10$  to 15 ka [thousand years ago]) [Scanlon, 1991; Phillips, 1994]. The Cl bulges have been attributed to a reduction in water fluxes during more arid conditions (xeric vegetation) in the Holocene (0 to 10–15 ka). There is an apparent inconsistency between the downward-flow assumption required by the

CMB approach to estimate water fluxes and upward flow suggested by the upward water potential gradients. This inconsistency was reconciled in some previous studies by assuming that the Cl data represented much longer timescales than the upward water potential gradients [Scanlon *et al.*, 1999]. From a waste-containment standpoint, assuming downward water fluxes provided a conservative estimate of water flux, and most interpretations assumed that the Cl bulges represented a reduction in water flux or zero water flux since the Pleistocene [Scanlon, 1991; Phillips, 1994; Prudic, 1994; Tyler *et al.*, 1996].

[6] The timescales represented by the upward water potential gradients were evaluated using numerical modeling by Walvoord *et al.* [2002] for typical arid interdrainage sites in the southwestern United States. A reversal in the direction of water movement from downward to upward was attributed to changes from mesic vegetation during Pleistocene pluvial periods to xeric vegetation during Holocene arid conditions [van Devender, 1990]. Downward water fluxes of 2–5 mm/yr, estimated from deep Cl concentrations, were simulated for the pluvial period ( $\geq 15$  ka). The transition to xeric vegetation was simulated by setting the matric potential head at  $\sim -400$  m at the base of the root zone ( $\sim 4$  m depth), which represents the ability of plants to capture infiltrated water in the root zone. These simulations demonstrated that downward propagation of drying fronts over time periods of  $\sim 15$  kyr would be required to reproduce the measured upward water potential gradients. The Cl bulges were simulated by downward diffusion of Cl driven by concentration gradients. Simulated current water fluxes at depth are much lower than the paleofluxes estimated using the CMB approach.

[7] The importance of vapor flow in semiarid and arid regions was evaluated by Ross [1984], who indicated that it should be very important in areas of little or no recharge ( $\leq 0.03$  mm/yr). In systems with no recharge, under isothermal conditions at steady state, the matric potential should balance the gravitational potential, resulting in a matric potential gradient of unity. Under nonisothermal conditions, upward vapor flow driven by the geothermal gradient would result in a matric potential gradient much less than unity. Conservation of mass would require a downward liquid flux to balance the upward vapor flux because thermal vapor flux varies with elevation. Ross [1984] predicted an upward vapor flux and corresponding downward liquid flux of 0.03 mm/yr for a system with a geothermal gradient of  $33^{\circ}\text{C}/\text{km}$ . The modeling studies by Walvoord *et al.* [2002] also indicate that upward geothermally driven vapor flow would provide water through condensation for upward isothermal liquid and isothermal vapor flow near the land surface and for downward liquid flow at depth.

[8] This study builds on previous work by evaluating water potential and Cl profiles at a number of semiarid and arid sites in the southwestern United States that represent different current climates, vegetation, and sediment textures. Detailed nonisothermal liquid and vapor flow simulations, similar to those conducted by Walvoord *et al.* [2002], were applied to the sites in this study to evaluate processes and controls on subsurface flow over millennia.

### 1.2. Site Descriptions

[9] The analysis of subsurface flow focuses on four different sites: the High Plains (HP) site near Amarillo in

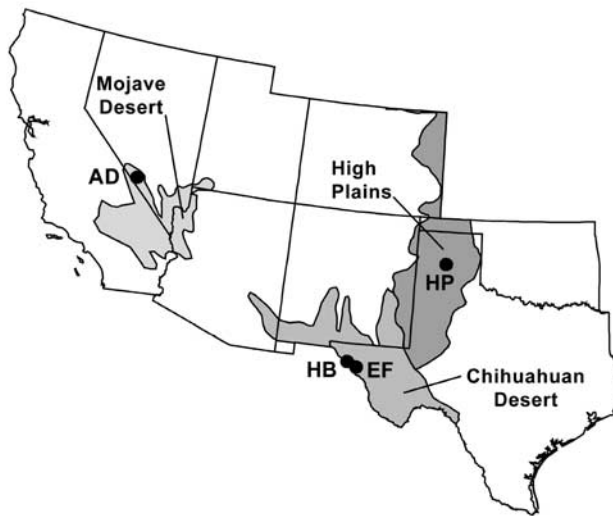


**Figure 1.** Study locations: Amargosa Desert site (AD) in the Mojave Desert, High Plains site (HP), and Hueco Bolson (HB) and Eagle Flat (EF) sites in the Chihuahuan Desert.

the Texas Panhandle; the Eagle Flat (EF) and Hueco Bolson (HB) sites in the Chihuahuan Desert in West Texas; and the Amargosa Desert (AD) site in the Mojave Desert near Beatty, Nevada (Figure 1 and Table 1). Detailed descriptions of these sites are given by Scanlon [1991, 1994], Andraski [1997], Scanlon and Goldsmith [1997], and Scanlon *et al.* [1999]. Sediment textures range from coarse grained (loamy sand (AD) and sand (shallow HB  $\leq 8$  m)) to fine grained (sandy clay loam (EF); clay loam (HP and deep HB ( $\geq 8$  m))) (Table 2). Long-term mean annual precipitation varies from 108 mm (AD) to 500 mm (HP) (Table 1). Vegetation is variable and is sparse at most sites (creosote bushes, AD; grasses, HP; grasses and shrubs, EF) and dense at the HB site (mesquite trees and creosote

**Table 2.** Soil Texture, Saturated Hydraulic Conductivity ( $K_s$ ), Saturated ( $\theta_s$ ) and Residual ( $\theta_r$ ) Water Content, and van Genuchten Parameters  $\alpha$  and  $n$ <sup>a</sup>

Site	Texture	Percent Sand, Silt, Clay	$K_s$ m/d	$\theta_s$ $m^3/m^3$	$\theta_r$ $m^3/m^3$	$\alpha$ , 1/m	$n$
HP/HB	clay loam	21,51,28	0.14	0.43	0.06	0.8	1.25
EF	sandy clay loam	56,23,21	0.41	0.35	0.04	0.8	1.21
HB	sand	92,7,1	5.87	0.38	0.03	5.0	1.95
AD	loamy sand	80,14,6	0.43	0.29	0.026	2.6	1.42

<sup>a</sup>Texture for the AD site represents the  $\leq 2$  mm fraction; the whole sample contained 22% gravel [Andraski, 1996] (Table 1). The HB profile consists of sand in the upper 8 m and clay loam at greater depth.

bushes). The water table depth varies from 75 m (HP) to 200 m (EF) (Table 1).

[10] Paleoclimate and paleovegetation of the different regions have been reconstructed from records of fluvial and lacustrine systems, speleothems (cave calcite formations), pollen, and packrat middens. Evidence of cooler and wetter conditions during the Pleistocene in the High Plains is provided by geologic records of water-filled playas and flowing streams. The transition to semiarid conditions on the High Plains during the Holocene is marked by a shift from erosion to deposition in fluvial channels and sediment aggradation (12 ka,  $^{14}\text{C}$  dating [Holliday, 1995]). Speleothems in Central Texas caves record up to two orders of magnitude higher growth rates from 24 to 12 ka (U series isotope dating), which were attributed to wetter conditions during the Pleistocene than during the Holocene [Musgrove *et al.*, 2001]. Information from paleolake shorelines within the Salt Basin in the Chihuahuan Desert in Texas reflects highstands ranging from 23 to 16 ka ( $^{14}\text{C}$  [Wilkins and Currey, 1997]). Packrat midden data record a shift from mesic pinon-juniper woodlands to xeric desert scrub containing creosote bushes and mesquite trees  $\sim 1\text{--}8$  ka [van Devender, 1990]. The paleoclimate near the Amargosa Desert has been reconstructed from lacustrine and marsh deposits and packrat midden data. Significantly wetter conditions from 150 and 120 ka and later from 24 and 10 ka caused Searles Lake (130 km southwest of the AD site) to overflow. Marsh deposits were recorded south of the AD site between 60 and 40 ka and between 30 and 15 ka [Quade, 1986]. Benson *et al.* [1990] and Morrison [1991] recorded variations in lake levels in western Nevada  $\sim 14\text{--}13$  ka. Packrat midden data record a shift in vegetation from mesic woodlands to xeric scrublands  $\sim 14\text{--}9$  ka in southern Nevada [Spaulding, 1990]. The paleoclimate and paleovegetation indicators are consistent and record cooler, wetter conditions during the Pleistocene and warmer, drier conditions during the Holocene.

## 2. Methods

[11] Detailed descriptions of the methods used at the HP, EF, and HB sites are given by Scanlon *et al.* [1991, 1999, 2000] and in Scanlon and Goldsmith [1997], and those for the AD site can be found in Fischer [1992], Prudic [1994], Andraski [1996, 1997], and Andraski and Prudic [1997]. Sediment samples from shallow excavations and deep boreholes were collected for laboratory analyses of sediment texture, bulk density, water content, water potential, and Cl concentration. Laboratory measurements of water potential

**Table 1.** Attributes for the High Plains (HP), Eagle Flat (EF), Hueco Bolson (HB), and Amargosa Desert (AD) Sites

	HP	EF	HB	AD
Precipitation (mm/yr) (30-yr average)	500	320	280	108
Water table depth (m)	75	200	150	110
Profile depth (wp) (m) <sup>a</sup>	22.1	19.3	24	47.5
Profile depth (Cl) (m) <sup>b</sup>	17.6	17.5	10.5	85
Cl precipitation (mg/L) <sup>c</sup>	0.3	0.27	0.29	1.6
Cl input (mg/m <sup>2</sup> /yr)	157	87	80	173
CMB flux base (mm/yr) <sup>d</sup>	1.3	0.04	0.2	8.4
Cl peak (mg/L)	2,515	6,575	9,343	9,000
Cl peak depth (m)	1.6	0.5	2.8, 4.7	2.3
Cl base (mg/L)	118	2,600	460	20
CMB age (kyr) <sup>e</sup>	9	12	13	16
CMB age base (kyr) <sup>f</sup>	9	90	17	18
Matric potential (root sink) (m) <sup>g</sup>	-250	-450	-450	-500
Root sink depth (m)	1.6	0.5	2.8	2.3
Geothermal gradient (°C/km)	25	25	35	40

<sup>a</sup>Depth of water potential profile.

<sup>b</sup>Depth of Cl profile.

<sup>c</sup>Cl concentration in precipitation and dry fallout.

<sup>d</sup>CMB flux at the base of the profile.

<sup>e</sup>CMB age at the base of the Cl bulge.

<sup>f</sup>CMB age at the base of the Cl profile.

<sup>g</sup>Matric potential assigned to root sink term in numerical model.

were made using a thermocouple psychrometer sample changer (SC10A; Decagon Devices, Inc., Pullman, WA) or a water activity meter (CX1; Decagon Devices Inc) [Andraski and Scanlon, 2002; Scanlon et al., 2002].

[12] In situ water potentials were monitored using thermocouple psychrometers (Model 74, J.R.D. Merrill Specialty Equipment, Logan, UT) [Andraski and Scanlon, 2002] installed in the sidewall of hand-dug pits ( $\sim 1.5$  m deep), in deep boreholes, and laterally out from an experimental instrument shaft. For each of the four sites, all samples and data were collected at locations that were in close proximity (i.e.,  $\leq 70$  m).

## 2.1. Numerical Modeling

[13] Numerical simulations were done to evaluate the timescales represented by upward water potential profiles. The simulations used a modified version of the HYDRUS-1D computer code [Simunek et al., 1998] that includes coupled liquid water, water vapor, and energy transport. The basic water flow equations are provided by Simunek et al. [1998]. Because vapor flow is discussed in detail in this study, the equations for vapor flow are provided here and are similar to those of Fayer [2000]. Liquid water flux is described by Darcy's law. Water vapor flux ( $q_v$ ) is described by Fick's law of diffusion:

$$\begin{aligned} q_v &= q_{vh} + q_{vT} = -K_{vh} \frac{\partial h}{\partial z} - K_{vT} \frac{\partial T}{\partial z} \\ &= -\frac{D}{\rho_w} \frac{Mg}{RT} H_r \frac{\partial h}{\partial z} - \frac{D}{\rho_w} \eta H_r \frac{\partial \rho_{vs}}{\partial T} \frac{\partial T}{\partial z} \end{aligned} \quad (1)$$

where  $q_{vh}$  is isothermal vapor flux ( $L T^{-1}$ ),  $q_{vT}$  is thermal vapor flux ( $L T^{-1}$ ),  $K_{vh}$  is isothermal vapor conductivity ( $L T^{-1}$ ),  $K_{vT}$  is thermal vapor conductivity ( $L^2 K^{-1} T^{-1}$ ),  $D$  is vapor diffusivity in soil ( $L^2 T^{-1}$ ),  $\rho_w$  is density of liquid water ( $M L^{-3}$ ),  $\rho_{vs}$  is saturated vapor density ( $M L^{-3}$ ),  $M$  is molecular weight of water ( $kg mol^{-1}$ ),  $g$  is gravitational acceleration ( $L T^{-2}$ ),  $R$  is gas constant ( $J mol^{-1} K^{-1}$ ),  $H_r$  is relative humidity,  $h$  is matric potential head (L),  $\eta$  is enhancement factor, and  $T$  is temperature (K). The vapor diffusivity in soil is

$$D = \tau \theta_a D_a = \frac{\theta_a^{7/3}}{\theta_s^2} \theta_a D_a; \quad D_a = 2.12 \times 10^{-5} \left( \frac{T}{273.15} \right)^2 \quad (2)$$

where  $\tau$  is tortuosity described by Millington and Quirk [1961],  $\theta_a$  is volumetric air content,  $D_a$  is diffusivity of water vapor in air ( $L^2 T^{-1}$ ), and  $\theta_s$  is saturated water content. HYDRUS-1D includes enhancements for thermal vapor flux as a result of liquid islands and increased temperature gradients in the air phase relative to the average temperature gradient [Philip and de Vries, 1957]. The Cass et al. [1984] formulation for the enhancement factor [Campbell, 1985] is used in HYDRUS-1D:

$$\eta = 9.5 + 3 \frac{\theta}{\theta_s} - 8.5 \exp \left( - \left( \left( 1 + \frac{2.6}{\sqrt{f_c}} \right) \frac{\theta}{\theta_s} \right)^4 \right) \quad (3)$$

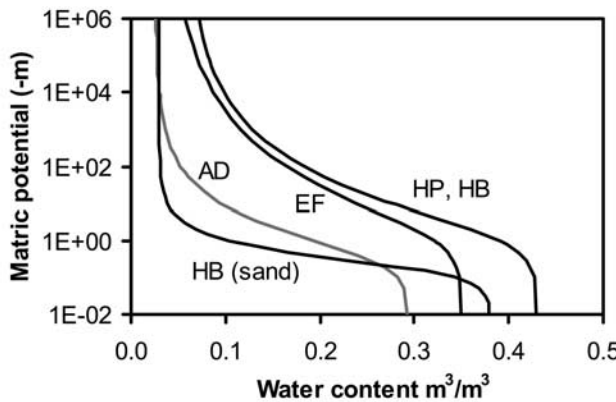
where  $f_c$  is mass fraction of clay in soil.

[14] The modeling approach used in this study was similar to that used by Walvoord et al. [2002]. The pluvial

period was approximated by simulating downward water fluxes, estimated from Cl concentrations beneath the bulge, until steady state was achieved. The resultant matric potentials provided initial conditions for simulations of the Holocene that included a constant head root sink at the base of the root zone to represent xeric vegetation. The base of the root zone was assumed equal to the depth of the Cl peak. The matric potential at the sink was assigned on the basis of measured water potentials just below the root zone (Table 1). The transient simulations therefore consisted of a step change from downward flux in the Pleistocene to upward flux during the Holocene. This simplified approach assumes that the assigned conditions are representative of long-term average conditions and avoids the complexities of simulating diurnally and seasonally varying water flux dynamics in the upper few meters, which were considered in previous studies [Scanlon and Milly, 1994]. The top boundary condition consisted of an applied water and solute flux equal to precipitation and Cl in precipitation and dry deposition. The entire unsaturated zone from the ground surface to the water table was simulated. The lower boundary condition was assigned zero pressure equal to the water table. The geothermal gradient was incorporated by specifying the temperature at the surface and in the groundwater. The surface temperature was set equal to the average temperature monitored at depths of 10 to 15 m, which is below the zone of seasonal fluctuations. In areas where accurate temperature data were not available, the geothermal gradient was estimated from the literature (HB site) [Henry and Gluck, 1981]. The grid cell size generally varied from 0.1 m at the surface to a maximum of 2 m within the profile and decreased to a minimum value of 0.05 m at the water table. Adaptive time stepping is used in HYDRUS-1D, and a minimum initial time step was generally set at 0.01 day. There was no limit on the maximum time step size.

## 2.2. Hydraulic Properties

[15] Profiles for most sites were represented using a single sediment type generally based on the dominant texture in the profiles, with the exception of the HB site, which was simulated using coarse-textured sand in the upper 8 m (Camp Rice Formation) underlain by clay loam (Fort Hancock Formation) that extends to the water table (150 m). Hydraulic properties were based on field or laboratory measurements of samples with the exception of the HB site. Hydraulic properties for the sand layer at the HB site were derived from the UNSODA database (UNSDA 4650 [Leij et al., 1996]), and the underlying clay-loam properties were based on measurements at the HP site. The AD site was represented by layer 1 material properties described in Andraski [1996]. Water retention measurements were made over a maximum pressure range of 0.2 to 18,000 m. Van Genuchten [1980] water retention functions were fitted to the laboratory-measured water retention data (Figure 2 and Table 2). The  $R^2$  values for measured versus fitted water contents ranged from 0.96 to 0.99. Unsaturated hydraulic conductivity was estimated from field or laboratory measurements of saturated hydraulic conductivity and water retention functions using the Mualem hydraulic conductivity model [Mualem, 1976] (Figure 3). The enhancement factors for thermal vapor diffusion for materials at each of the sites are shown in



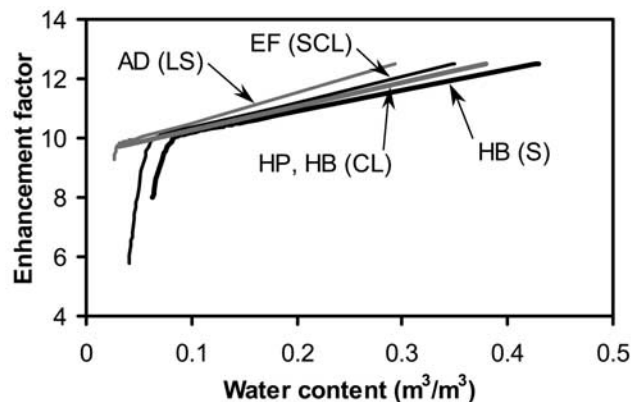
**Figure 2.** van Genuchten water retention functions for sediment textures used to model each site. Values for van Genuchten parameters are listed in Table 2.

Figure 4. Thermal conductivity for each sediment texture as a function of water content was based on data from *Chung and Horton* [1987].

### 3. Results and Discussion

#### 3.1. Water Potential Monitoring

[16] Long-term (5 to 12 yr) monitoring of water potentials at each site indicates that penetration of wetting fronts in



**Figure 4.** Enhancement factors for different sediment textures (LS, loamy sand; SCL, sandy clay loam; CL, clay loam; S, sand) at the High Plains (HP), Eagle Flat (EF), Hueco Bolson (HB), and Amargosa Desert (AD) sites. Water content ranges from saturated to residual for each texture.

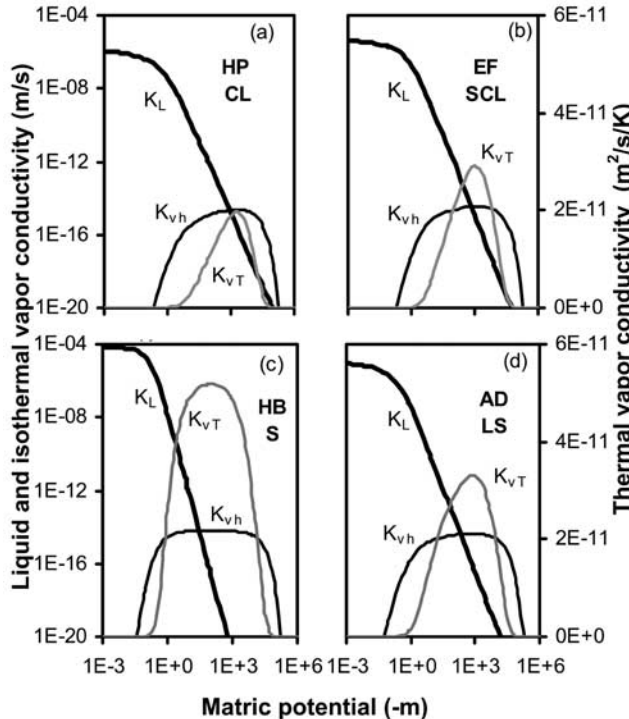


**Figure 3.** Liquid ( $K_L$ ), isothermal vapor ( $K_{vh}$ ), and thermal vapor ( $K_{vT}$ ) conductivity calculated by HYDRUS-1D for sediment textures at each site. Hueco Bolson sand properties represent the upper 8 m depth, and clay loam at greater depth is represented by the High Plains properties. (CL, clay loam; SCL, sandy clay loam; S, sand; LS, loamy sand).

response to seasonal and annual fluctuations in precipitation is restricted to the shallow subsurface. The wetting front is defined as water potential close to zero. Wetting fronts penetrated to a maximum depth of <0.3 m (EF), 0.8 m (HB), 1.2 m (AD), and 2.9 m (HP) (Figure 5). Deeper penetration of water at the HB site compared with the EF site in the Chihuahuan Desert is attributed to coarser textured soils at the HB site (Table 1). Infiltration occurs primarily in response to winter precipitation at all sites and also in response to summer monsoonal precipitation in the Chihuahuan Desert (EF and HB sites). Winter infiltration often results in water potential increases for several months because ET is low. Rapid removal of this water generally occurs in the spring in response to increased ET. In contrast, the duration of summer increases in water potential is much shorter ( $\leq 1$  month) because ET rates are high. Temporal variability in water potentials at each site reflects the complex interplay between seasonal changes in climate forcing, sediment texture, and vegetation.

[17] Data from most sites indicate predominantly piston flow with progressive increases in water potential with depth after precipitation events. Water potential increases in a gravel layer at 1.2 m depth at the AD site during high precipitation in 1987 are attributed to preferential flow down the instrument borehole because water potentials increased at this depth prior to those at shallower depths. Data from the HP site also suggested that preferential flow might have resulted from instrument installation. Water potentials were low during the first 3 years, suggesting dry conditions. Water potential fluctuations then became spiky at depths of 1.7 to 2.9 m, suggesting preferential flow. Ultimately water potentials at these depths remained uniformly high, indicating percolation of water to these depths; however, coring and analysis of Cl profiles in a nearby borehole after this time indicated steadily increasing Cl concentrations from an average value of 40 mg/L in the top meter to a peak value (1550 mg/L) at 4 m depth. Heat-dissipation sensors were also installed within a 2-m radius of the original thermocouple psychrometer installations and indicated much lower matric potentials in the upper 6 m

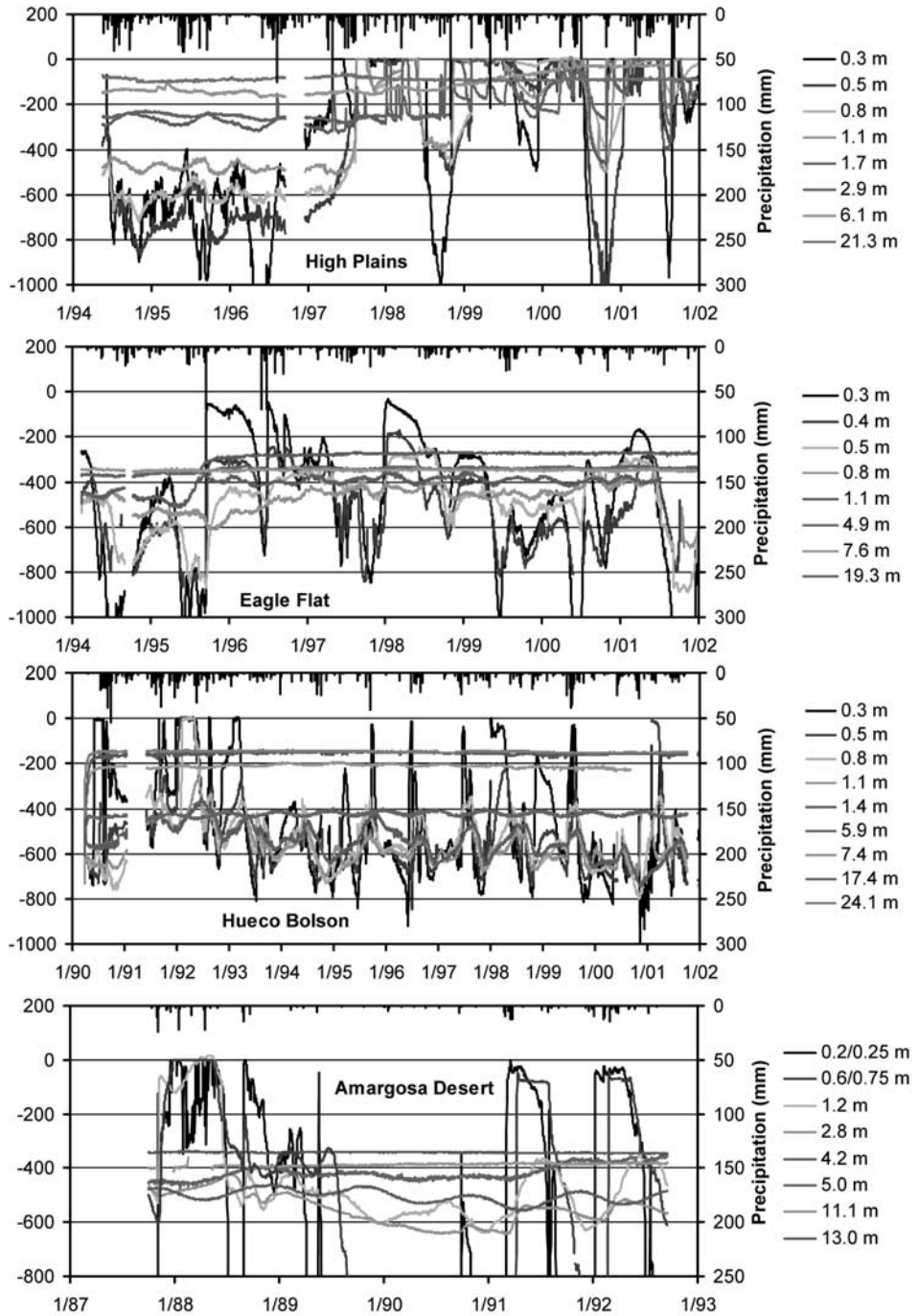


**Figure 5.** Temporal variability in water potential monitored in situ at various depths at each site. Daily precipitation is also shown. See color version of this figure at back of this issue.

than the thermocouple psychrometer data. These results underscore the difficulties of monitoring structured soils without artificially creating preferential pathways.

[18] Temporal variations in water potential decrease with depth. Seasonal water potential fluctuations occur to depths of  $\sim 5$  to 7 m and can be seen most clearly in data from the HB site. These fluctuations are attributed to seasonal temperature fluctuations similar to those recorded in another nearby profile [Scanlon, 1994]. Large seasonal fluctuations in water potentials at the AD site (e.g., 1.2 m depth) could not be explained by temperature effects on water potential

and were attributed to seasonality of vapor fluxes [Andraski and Jacobson, 2000].

### 3.2. Comparison of Field- and Laboratory-Measured Water Potentials

[19] Many previous studies of flow in semiarid and arid regions are based on laboratory-measured water potentials [Prych, 1998; Izbicki *et al.*, 2000; Walvoord, 2002]; however, these measurements may be biased because of the possibility of sample drying during field collection. Field monitoring should accurately record in situ water potentials.

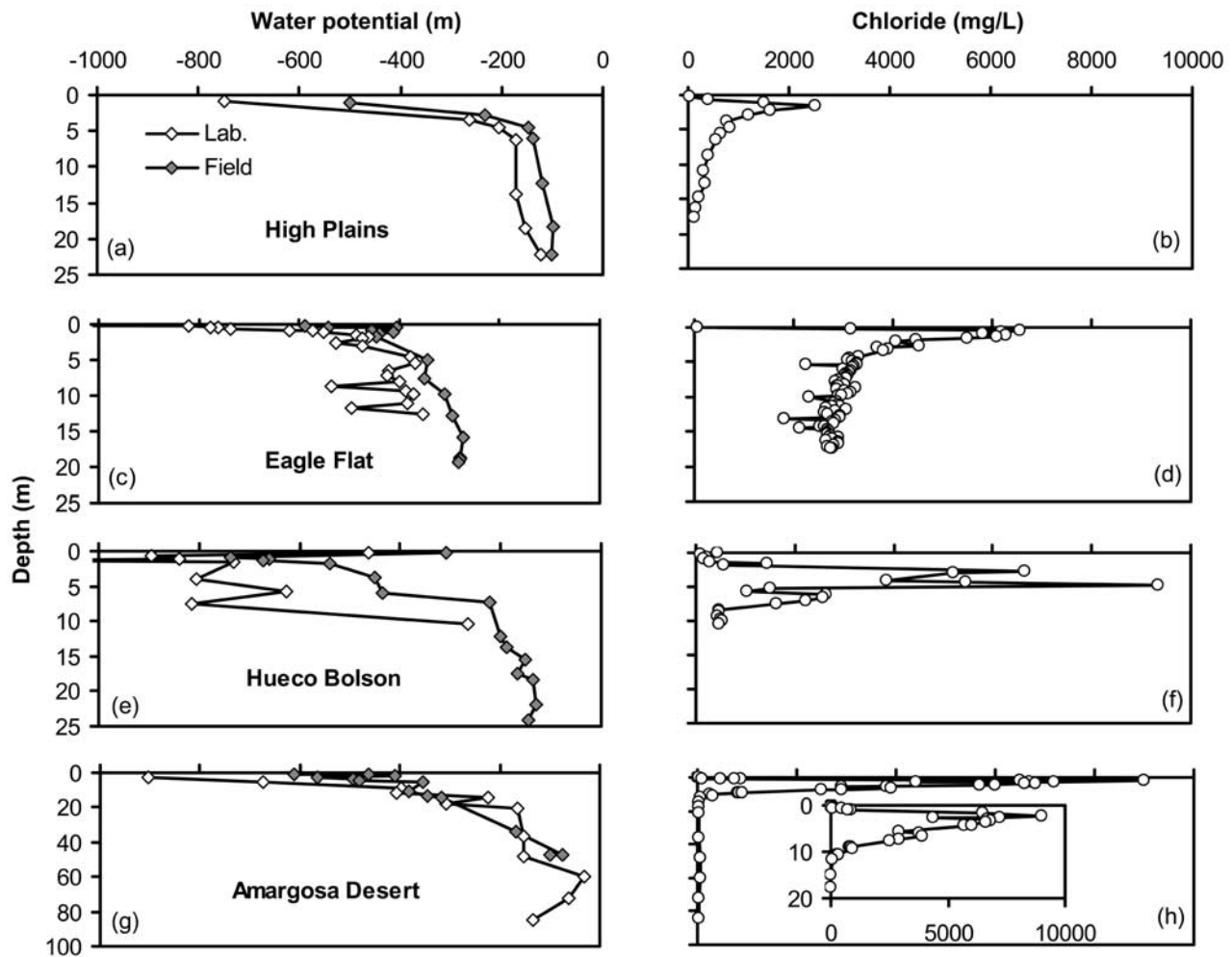


**Figure 6.** Water potential profiles (laboratory measured and field monitored) and Cl concentration profiles for each site. The inset in the Amargosa Desert Cl profile shows more detail in the upper 20 m zone.

Comparison of laboratory- and field-measured water potentials indicates that the trends in both are similar; lowest water potentials at the surface indicate very dry conditions, and exponentially increasing water potentials with depth indicate progressively wetter conditions (Figure 6). However, laboratory-measured water potentials were generally lower (more negative) than field-measured water potentials. Water loss from coarse-textured and low water content soils can be most problematic because a small change in water content can result in a large change in water potential. Laboratory- and field-measured water potentials (Figure 6) indicate that core drying can result in errors as great as 250 to 600 m.

### 3.3. Chloride Profiles

[20] All Cl profiles are bulge shaped with low Cl concentrations near the surface, increasing to peak concentrations that ranged from 2,515 mg/L (1.6 m depth, HP) to 9,343 mg/L (4.7 m depth, HB), and decreasing to lesser concentrations of 20 mg/L (AD) to ~2,600 mg/L (EF) (Figure 6). The low Cl concentrations near the surface are attributed to leaching of Cl by seasonal infiltration. Peak Cl concentrations were lowest in the semiarid HP site and

much higher in the arid sites. Peak Cl concentrations at the AD and HB sites were similar (~9000 mg/L). The Cl profile at the HB site is multipeaked. Cl concentrations at depth were one to two orders of magnitude lower than peak values, with the exception of the EF site, which has high Cl concentrations at depth (~2600 mg/L).

[21] The bulge-shaped Cl profiles have generally been interpreted as representing accumulation of Cl since the Pleistocene (Figure 7). Total profile CMB ages were calculated using the best available estimates of average Cl input during the Holocene. CMB ages for the entire profile ranged from 9 to 18 kyr for HP, AD, and HB sites (Table 1). In contrast, CMB age for the EF site was much higher (90 kyr). This high CMB age raises the question about whether there are additional sources of Cl at the EF site. The EF site is located ~25 km southwest of a Salt Flat playa; however, Cl/Br ratios (92–150) in subsurface profiles are similar to Cl/Br ratios in precipitation at this site (24–167) and are typical of meteoric Cl [Davis *et al.*, 1998]. Cl/Br ratios in samples affected by halite dissolution typically range from 1000 to 10,000 [Davis *et al.*, 1998]. Cl/Br ratios remain fairly uniform with depth at the EF site (Figure 8). Prebomb  $^{36}\text{Cl}/\text{Cl}$  ratios in different profiles at the EF site (383 ×

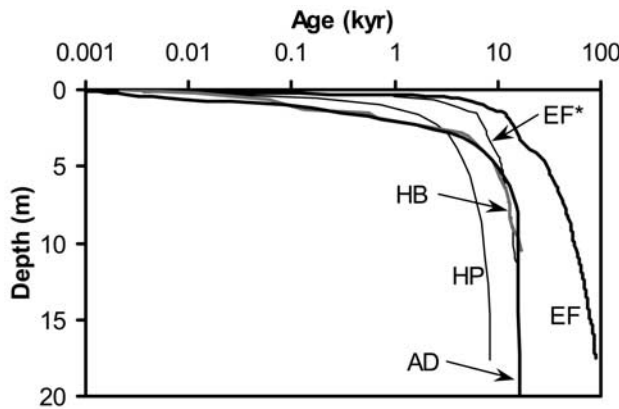


**Figure 7.** Chloride mass balance age versus depth for profiles at the Hueco Bolson (HB), High Plains (HP), Amargosa Desert (AD), and Eagle Flat (EF) sites. EF\* represents Eagle Flat profile after the background concentration of 2800 mg/L was subtracted from shallow bulge.

$10^{-15}$  to  $723 \times 10^{-15}$ ) are significantly higher than those in the Salt Flat ( $\sim 90 \times 10^{-15}$ ) and suggest that Cl input from the Salt Flat is unlikely [Scanlon, 2000]. A Cl bulge can be identified in the EF profile, and the Cl inventory of this bulge was estimated by subtracting the background concentration of 2600 mg/L from the Cl concentrations. The CMB age of this bulge is  $\sim 12$  kyr, which is similar to the ages estimated for the bulges in the other profiles (9 kyr, HP to 16 kyr, AD) (Table 1).

[22] Water fluxes were estimated from Cl concentrations below the Cl bulge and range from 0.04 mm/yr (EF) to 8.4 mm/yr (AD) (Table 1). These water fluxes are interpreted to represent fluxes during the cooler, wetter climate of the Pleistocene for most profiles and much longer time periods for the EF site ( $\sim 12$  to 90 kyr). Water fluxes were highest at the AD (8.4 mm/yr) and HP (1.3 mm/yr) sites, which may reflect wetter conditions during the Pleistocene at these sites relative to the Chihuahuan Desert sites. The proximity of the EF and HB sites in the Chihuahuan Desert suggests that the paleoclimatic forcing at these two sites should have been similar. The difference in Pleistocene water fluxes between the two sites (EF, 0.04 mm/yr; HB, 0.2 mm/yr) may be attributed to coarser grained sediments at the HB site, which allowed this system to respond much more to wetter conditions during the Pleistocene than did the EF site. This negligible response to Pleistocene conditions at the EF site is also consistent with the shallowest penetration of the wetting front at the EF site under current climatic forcing (Figure 5). These data demonstrate the importance of sediment texture in controlling system response to paleoclimatic forcing.

### 3.4. Numerical Modeling

#### 3.4.1. Simulated Versus Measured Water Potential and Cl Profiles

[23] Simulated matric potential profiles agree reasonably well with measured water potential profiles (Figure 9). The wet initial conditions corresponding to mesic vegetation during the Pleistocene pluvial period were based on downward simulations of water fluxes estimated from Cl concentrations beneath the bulge. A constant matric potential

sink was assigned to the base of the root zone to represent the transition to xeric vegetation during the Holocene period, which is approximated by the CMB age at the base of the Cl bulge at each site (Table 1). Simulated matric potentials are similar to current measured water potentials at the end of this time period. The time required to reproduce the measured water potential profile at the HP site ( $\sim 1$ –2 kyr) is much shorter than the CMB age at the base of the Cl bulge ( $\sim 9$  kyr) at this site. Simulated matric potentials at the EF site overestimate measured water potentials but are similar to estimated matric potentials from field data calculated by subtracting the osmotic potential. These data are discussed in more detail in section 3.5.2. Simulated matric potentials and measured water potentials at the HB site are similar in magnitude; however, the simulated minimum matric potential is deeper than the measured minimum because the depth of the root zone was based on the peak Cl concentration. The simulations of the AD site overestimate measured water potentials, even after 16 kyr of upward flow related to xeric vegetation.

[24] There is also fairly good agreement between simulated and measured Cl profiles. Simulations of the HP, EF, and AD sites underestimate the Cl peak by up to 25%, whereas simulations of the HB site overestimate the peak by 75%. Simulated Cl concentrations at depth below the peak underestimate measured values at the HB site. The Cl bulges result primarily from addition of Cl to the system from precipitation, with the exception of the EF site, where upward flow from depth contributes about 70% of the Cl to the bulge because of the high Cl concentrations at depth. Because water movement is upward below the root sink, diffusion driven by the concentration gradient is the only process that can transport Cl below the sink. These results demonstrate that it is possible to generally reproduce measured water potential and Cl profiles by simulating the transition from mesic to xeric vegetation and associated upward flow for long time periods (1–16 kyr).

[25] Cl bulges are excellent indicators of low water flux, and their formation process is similar to that of calcic soils. Both Cl profiles and calcic soils indicate low water flux; however, Cl is much more readily flushed out of the soil profile under increased downward fluxes than calcium carbonate, which can remain in a relict calcic horizon for

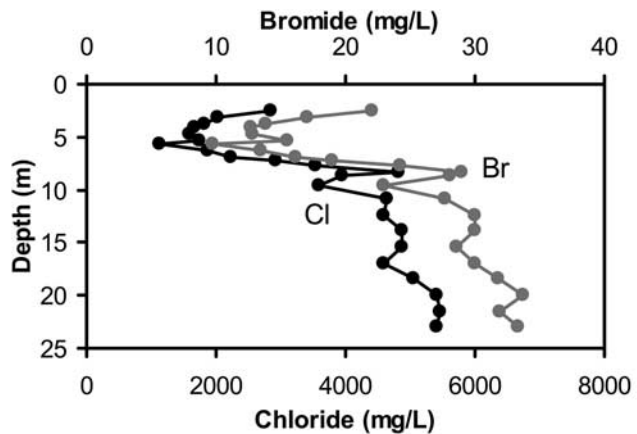


**Figure 8.** Chloride and bromide concentrations in an EF site profile.

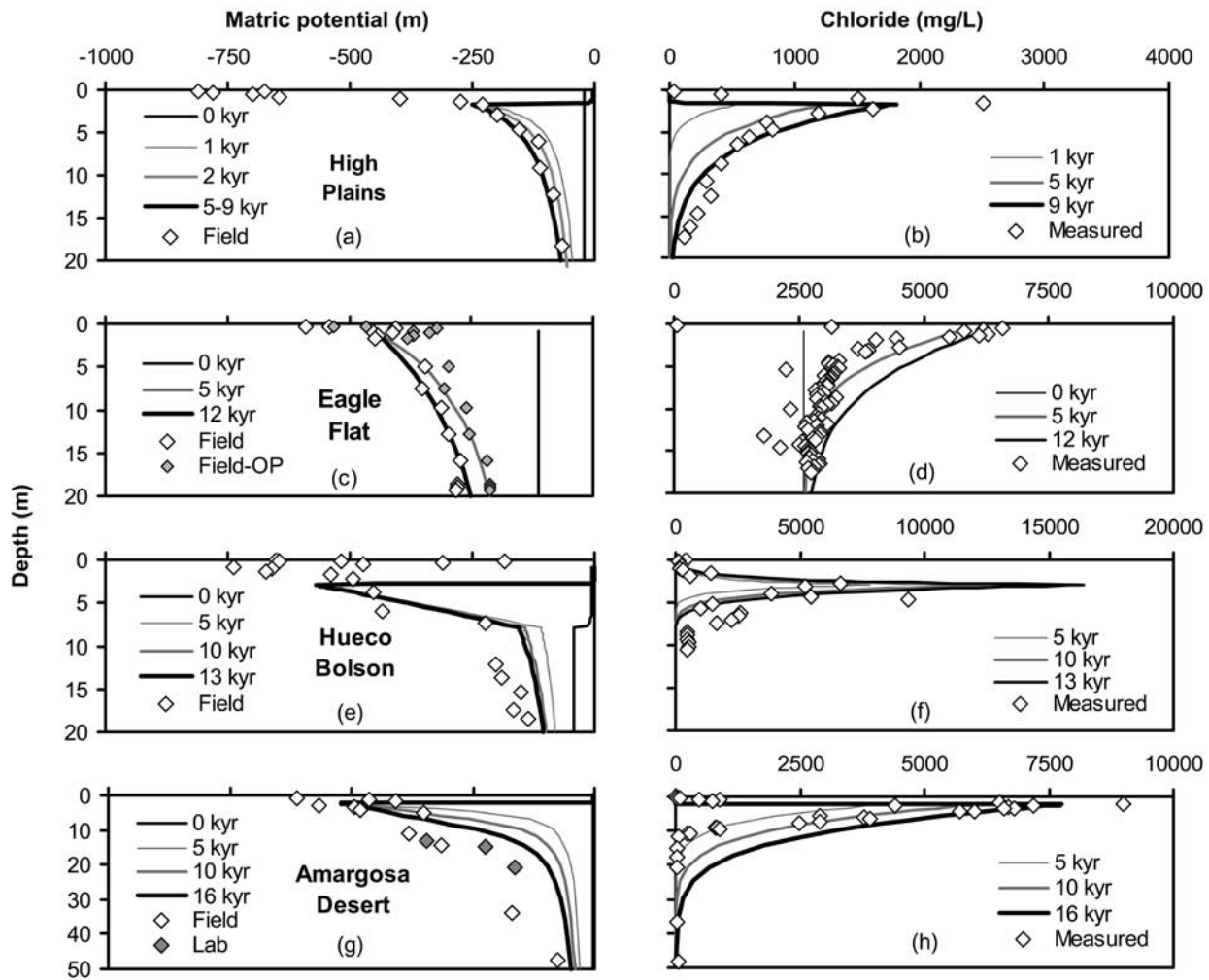


**Figure 9.** Simulated matric potentials and Cl concentrations for each site. Time 0 kyr represents wet initial conditions (Pleistocene pluvial period). The remaining times represent different periods of upward flow to a maximum time based on CMB age at the base of the Cl bulge for each site. Measured water potential and Cl profiles are shown for comparison with simulated profiles. Estimated matric potentials are also shown for the EF site after subtracting the osmotic potential (Field - OP). Laboratory-measured water potentials are also included in the AD profile to fill a gap in the field-measured data.

a long time. This can be shown by flushing of the AD Cl profile with a flux of 10 mm/yr (Figure 10). The Cl bulge moves deeper with time, and the peak concentration decreases with time. After 2000 yr, the Cl bulge was completely flushed out of the profile.

#### 3.4.2. Relative Importance of Liquid and Vapor Flow

[26] Simulated water-flux profiles for each site reveal differences in flux regimes among the sites (Figure 11). All of the simulations include enhanced vapor flux. Total water flux includes liquid and vapor flux components. The flux profiles at the HP site show propagation of the drying front with time (Figure 11a). Vapor flux is negligible at this site; therefore liquid water and total water (liquid + vapor) fluxes are approximately equivalent. After 1 kyr of drying, total water flux is divergent, with upward water flux (positive) in the top ~25 m controlled by matric potential forces and downward water flux (negative) at greater depth

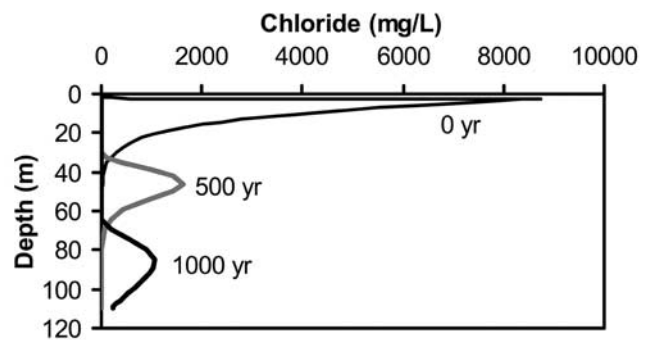


**Figure 10.** Flushing of Cl caused by a downward water flux of 10 mm/yr. The 0 yr profile represents the measured Cl concentration at the AD site.

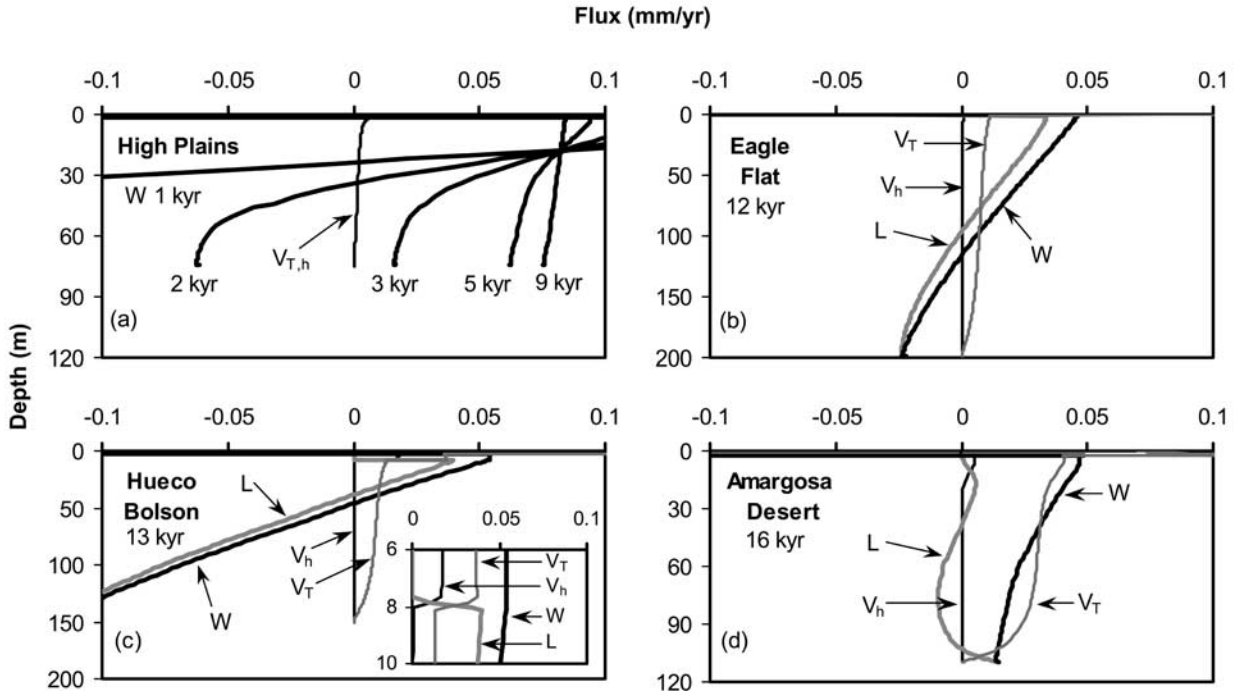


**Figure 11.** Simulated total water (W), liquid (L), isothermal ( $V_h$ ), and thermal ( $V_T$ ) vapor flux profiles that represent current conditions after drying for different time periods since Pleistocene pluvial conditions. Downward fluxes are negative and upward fluxes are positive. The propagation of the drying front is shown for the HP site by including results after 1, 2, 3, 5, and 9 kyr of drying. Liquid flux at the HP site is approximately equal to total water flux.

controlled by gravity. The plane of divergence can exist in the profile because of the transient nature of flow. The plane of divergence reaches a depth of  $\sim 35$  m after 2 kyr of drying. After  $\sim 3$  kyr of drying the plane of divergence has reached the water table, and water flux is upward throughout the entire profile. The profile has almost reached steady state after 9 kyr of drying with a uniform upward water flux of  $\sim 0.08$  mm/yr. This upward flux differs in magnitude and direction from the water flux estimated according to the CMB approach (1.3 mm/yr downward).

[27] The total water flux profile at the AD site after 16 kyr of drying is upward throughout the unsaturated zone (Figure 11d). Simulated total water flux at the base of the profile is  $\sim 0.01$  mm/yr upward, which is in the opposite direction and much lower than the downward CMB flux of 8.4 mm/yr. In contrast to the HP site, vapor flux is dominant at the AD site. Thermal vapor flux is dominant throughout most of the profile, whereas isothermal vapor flux is negligible except near the surface where matric potential gradients are steep. Thermal vapor flux is fairly uniform throughout much of the profile ( $\sim 0.03$  mm/yr) and decreases to zero at the water table because the sediments become saturated. Liquid water flux is upward in the upper  $\sim 40$  m, controlled by matric potential gradients, and generally downward at greater depth, controlled by gravity.

[28] The plane of divergence for total water flux is within the unsaturated zone for the two deeper profiles (EF and HB) in the Chihuahuan Desert (Figures 11b and 11c). The plane of divergence of total water flux is  $\sim 115$  m deep in

the EF profile after 12 kyr of drying. Liquid flux is upward in the upper 95 m as a result of matric potential gradients and downward below 95 m as a result of gravity. Thermal vapor flux is upward throughout the profile and ranges from 0 at the water table to 0.01 mm/yr near the surface. The flux profiles at the HB site are similar to those at the EF site except that the planes of divergence of liquid and total water flux are shallower ( $\sim 40$ –45 m deep). Vapor flux is dominated by thermal vapor flux, which ranges from 0 at the water table to 0.01 mm/yr at the base of the shallow sand zone (8-m depth). Isothermal and thermal vapor fluxes increase in the sand zone by a factor of  $\sim 2$  to 4, whereas liquid water flux decreases to  $\sim 0$ . Simulated downward water fluxes at the base of the EF and HB profiles (0.02 and 0.13 mm/yr, respectively) are less than the CMB-calculated fluxes (0.04, 0.2 mm/yr).

[29] The magnitude of vapor fluxes varied among sites. Negligible vapor fluxes at the HP site are attributed to high water contents associated with fine-grained sediments and to the higher matric potential assigned to the root sink (Table 1). Although sediments at the HP site are similar to those at the HB site below the sand zone, vapor fluxes are higher at the HB site because the matric potential at the root sink is much lower at this site relative to the HP site. Vapor fluxes are similar in the fine-grained sediments at the HB and EF sites. High vapor fluxes in the upper 8 m at the HB site and throughout the AD profile are attributed to coarse-grained sediments and extremely low water contents.

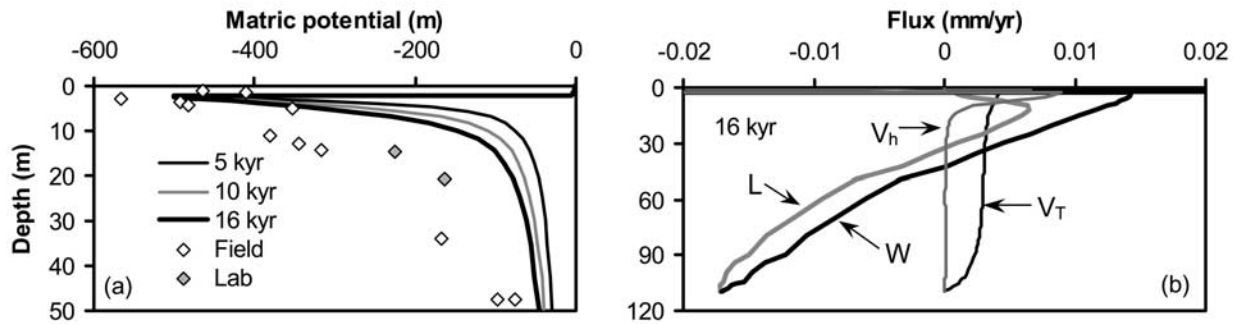


**Figure 12.** Simulated matric potentials and fluxes (total water (W), liquid (L), isothermal ( $V_h$ ), and thermal ( $V_T$ ) vapor) for unenhanced vapor flux at the AD site. For comparison with enhanced vapor flux, see Figure 9g for simulated water potential and Figure 11d for simulated fluxes. Field- and laboratory-measured water potentials are also shown.

[30] The effect of the enhancement factor on thermal vapor diffusion was evaluated in simulations of the AD profile where vapor flux was highest throughout the profile. The enhancement factor increases with water content (Figure 4). Neglecting the enhancement factor in simulations resulted in up to 30% higher (less negative) matric potentials and much lower thermal vapor fluxes by almost an order of magnitude (Figure 12). Similar results were found at the EF site. The flux regime for the AD site changes from upward total water flux throughout the profile under enhanced vapor-flux conditions (Figure 11d) to a divergent flux regime at 35-m depth under unenhanced vapor-flux conditions (Figure 12b). Simulated CI profiles were similar for enhanced and unenhanced vapor flux.

[31] With the exception of the HP site, which almost reached steady state after  $\sim 9$  kyr of drying, none of the other profiles had reached steady state at the end of the drying period (Figure 11). To evaluate steady state fluxes, a simpler simulation was conducted with a constant pressure head at the surface equal to that assigned to the root sink. Pressure and flux profiles are shown for the EF and AD sites (Figure 13). The flux profile had almost reached steady state after 60 kyr of drying at the EF site and after 100 kyr of drying at the AD site. However, it is unlikely that these profiles will ever reach steady state in the natural system because the timescales for climate change ( $\sim 10$  kyr) are much shorter than the time required to reach steady state. Total water flux is upward throughout the profile at steady state (EF  $\sim 0.03$  mm/yr; AD  $\sim 0.05$  mm/yr). Liquid water fluxes decrease with elevation above the water table as the sediments become drier. Decreasing upward liquid water fluxes are balanced by increasing upward thermal vapor fluxes. Thermal vapor fluxes were expected to decrease with elevation above the water table because temperature decreases with elevation; however, the effect of decreasing water content on thermal vapor conductivity ( $K_{VT}$ ) outweighs the effect of decreasing temperature in these profiles. For example, the change in  $K_{VT}$  with water content throughout much of the AD profile (water content  $0.040\text{--}0.075 \text{ m}^3 \text{ m}^{-3}$ ,  $T = 24^\circ\text{C}$ ) was about two times greater than the change in  $K_{VT}$  with temperature ( $22\text{--}26^\circ\text{C}$ ; water content  $0.06 \text{ m}^3 \text{ m}^{-3}$ ). Isothermal vapor fluxes are negligible throughout both profiles at steady state.

[32] Flux profiles described in this study were compared with typical flux profiles that were described by Walvoord *et al.* [2002] using the deep arid system hydrodynamics (DASH) model for the southwestern United States. Vapor flow was considered an integral part of the DASH model; however, in this study it was found that fine-grained sediments and wetter conditions at the HP site resulted in negligible vapor flux. The flux profile at the AD site after 16 kyr of drying without enhanced vapor flux (Figure 12b) is most similar to the typical profile described by the DASH

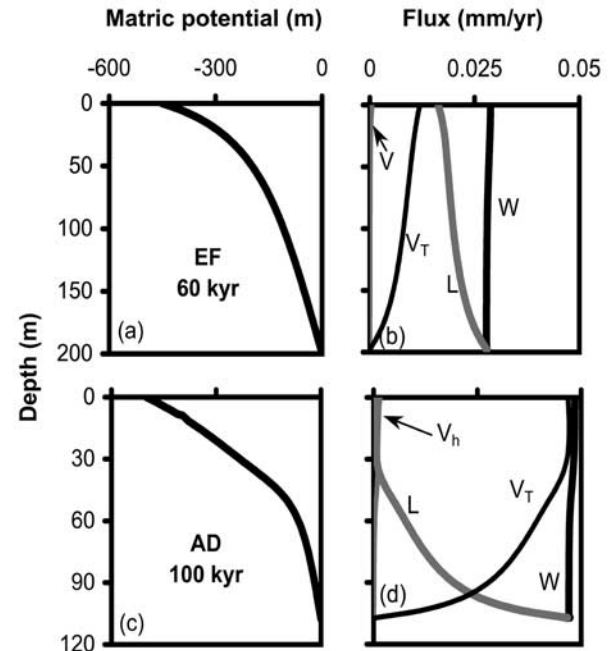


**Figure 13.** Simulated matric potentials and fluxes (W, total water flux; L, liquid water flux;  $V_T$ , thermal vapor flux;  $V_h$ , isothermal vapor flux) at steady state at the EF and AD sites. Matric potentials in equilibrium with the gravitational potential field under isothermal conditions are shown for comparison with simulated matric potentials.

model because both profiles have coarse-grained sediments and matric potentials at the root sink are similar. The steady state flux profile for the AD site, however, differs significantly from the steady state base case profile for the DASH model simulated using the FEHM code. The differences cannot be attributed to the use of different codes because the patterns in fluxes and heads in the DASH base case could be reproduced using HYDRUS-1D that used unenhanced vapor flux. The differences in flux profiles between the two sites can be attributed to differences in water retention functions. Thermal vapor flux at the AD site is dominated by the effect of water content, which decreases by up to a factor of 2 with elevation throughout much of the profile and results in increasing thermal vapor flux with elevation. In contrast, water content remains fairly uniform with elevation in the DASH base case; therefore temperature is the dominant driving force for thermal vapor flux, which decreases with elevation as temperature decreases and is balanced by downward liquid water flux at depth. This comparison underscores the difficulties of developing general profiles because of variability in climatic conditions and hydraulic properties from site to site.

### 3.5. Uncertainty Analysis

[33] Evaluation of uncertainties is important in order to identify gaps in our knowledge and areas of future research. Uncertainty analysis conducted by *Walvoord et al.* [2002] addressed the effects of varying water table depths, saturated hydraulic conductivities, geothermal gradients, and vapor diffusion enhancement. The current study builds on the uncertainty analysis of *Walvoord et al.* [2002] and addresses uncertainties in CMB ages, osmotic component of water potentials, and numerical modeling. Uncertainties in numerical modeling include those related to conceptual models, hydraulic parameterization, and solute diffusion coefficients. Improving understanding of these uncertainties is critical to evaluating subsurface flow and transport in response to paleoclimatic forcing.

#### 3.5.1. Chloride Mass Balance Ages and Fluxes

[34] In assessing the response of subsurface flow and transport to past climate fluctuations, we rely on the chloride mass balance (CMB) approach to determine the age of the water and to compare water fluxes during different climatic conditions. The Pleistocene/Holocene climate and associated vegetation transition generally occurred about 10 to 15 ka. CMB ages for the base of the Cl bulges vary from ~9 kyr for HP to 16 kyr for AD (Table 1). Water fluxes (0.04–8.4 mm/yr) were also estimated from Cl concentrations beneath the bulge representing the Pleistocene. What are the uncertainties in these CMB ages and fluxes? Uncertainties in various parameters in the CMB equation linearly translate to uncertainties in calculated ages and fluxes because the equations for estimating ages and fluxes are linear. Detailed analysis of uncertainties related to the CMB approach is described by *Scanlon* [2000]. In this section, we focus on uncertainties in Cl input, which was estimated from prebomb  $^{36}\text{Cl}/\text{Cl}$  ratios for the HP, EF, and HB sites [*Scanlon*, 1991, 2000; *Scanlon and Goldsmith*, 1997]. Uncertainty in these estimates has previously been assigned  $\pm 35\%$  [*Scanlon*, 2000]. Accurate estimates of Cl input are not available for the AD site. The CMB age previously estimated at the base of the AD site's Cl bulge

(16.5 kyr [*Phillips*, 1994]) was based on incorrectly calculated Cl concentrations [*Fouty*, 1989] that differed from true Cl concentrations by a factor of 1.7 (bulk density of the soil) [*Prudic*, 1994]. Applying the same Cl input (100 mg/m<sup>2</sup>/yr) used by *Phillips* [1994] with the correct Cl concentrations would result in an age of 28 kyr. If we assume that the Cl bulge generally represents accumulation after the Pleistocene, a CMB age of ~16 kyr would require a Cl input of 173 mg/m<sup>2</sup>/yr. This Cl input value is similar to the upper range of values suggested by *Prudic* [1994] and may reflect additional Cl from run-on. Increasing the Cl input will also increase the estimated water flux during the Pleistocene.

[35] Estimation of Cl inputs in many areas has been somewhat arbitrary. For example, the Cl input at Frenchman Flat at the Nevada Test site was increased by a factor of 1.5 to account for increased precipitation during the Pleistocene [*Tyler et al.*, 1996]; however, this increased input has also been applied to the Holocene record, which would underestimate the age of the Pleistocene/Holocene transition by 1.5. Cl inventories estimated from Cl bulges generally are locally variable. For example, profiles in interstream settings in the Hueco Bolson have inventories that correspond to ages of 13 to 25 kyr at the base of the Cl bulge [*Scanlon*, 1991]. *Walvoord* [2002] also noted differences in Cl inventories of up to a factor of two in a study of the Trans-Pecos region in Texas. This variability may reflect variations in input related to subtle differences in topography or run-on. CMB ages may not be sufficiently accurate to locate the Pleistocene/Holocene transition; however, the Cl bulges in many cases can generally be assumed to correspond to Cl accumulation during the Holocene and appropriate ages calculated by varying the Cl input within the range of uncertainties.

#### 3.5.2. Osmotic Component of Water Potential

[36] Thermocouple psychrometers at each site monitor water potentials, which include matric and osmotic potentials. However, the HYDRUS-1D code simulates only matric potentials and does not include osmotic potentials. Isothermal vapor flux driven by osmotic potentials was estimated for the AD site, which has the steepest Cl concentration gradient (Figure 6h). Osmotic potentials were estimated from the Cl concentration data [*Campbell*, 1985; *Scanlon*, 1994] and the gradient resulted in an isothermal vapor flux that was about an order of magnitude less than the average isothermal vapor flux driven by the matric potential gradient in this zone. Simulated isothermal vapor fluxes driven by matric potentials are close to zero at most sites; therefore osmotically driven vapor fluxes are negligible. However, osmotic potentials also affect the simulated time required to reproduce the measured water potentials and ignoring osmotic potentials may result in overestimation of this time.

[37] It is difficult to estimate osmotic potentials. Estimates of osmotic potentials based on Cl concentrations should provide a lower boundary on osmotic potentials because many more ions are in solution than Na and Cl. Osmotic potentials based on NaCl data at the sites examined in this study are generally less than 10 to 20% of the measured water potentials because the depths where osmotic potentials are most negative generally correspond to the depths where water potentials are also most negative [*Fischer*, 1992; *Scanlon*, 1994]. Osmotic potentials may be

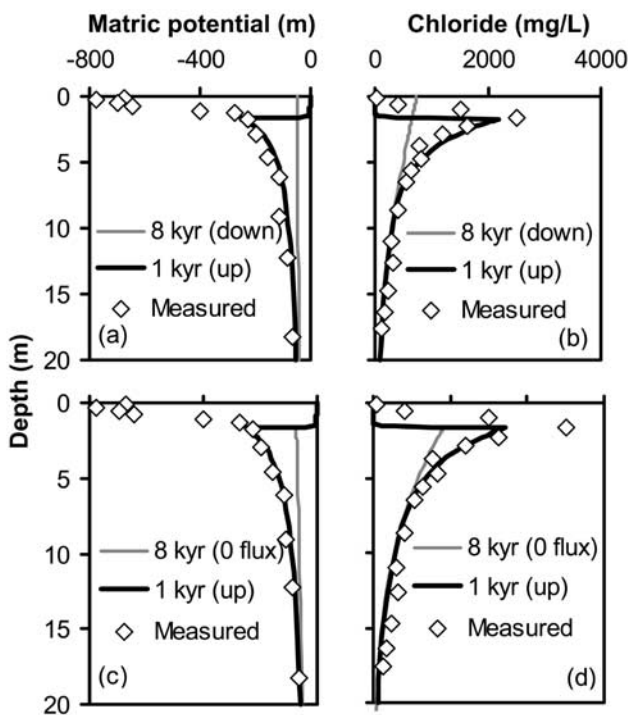


**Figure 14.** Alternative conceptual models for simulating measured water potentials and Cl profiles at the HP site. Simulations based on downward flux  $\sim 0.1$  mm/yr (a and b) and zero flux (c and d) for 8 kyr followed by upward flux for 1 kyr are shown. Measured water potentials are also shown.

important at the EF site where Cl concentrations at the base of the profile are  $\sim 2600$  mg/L (Figures 9c and 9d). Studies by Izbicki *et al.* [2000] indicate that osmotic potentials calculated using only NaCl data differ from those based on total ion chemistry by a factor of  $\sim 4$ . Differences in measured water potentials between HB ( $-140$  m) and EF ( $-300$  m) sites at depth may be explained by osmotic potentials if we increase, by a factor of 4, the osmotic potentials based on NaCl ( $-40$  m) for the EF site. Osmotic potentials are difficult to estimate accurately because soil-solution samplers do not function at these low water potentials and it is difficult to extract water using centrifugation. The effect of bound water may also be important.

### 3.5.3. Numerical Modeling

#### 3.5.3.1. Conceptual Model Uncertainty

[38] The conceptual model used in this study is relatively simple and assumes downward water flux associated with mesic vegetation during the Pleistocene and upward water flux near the root zone associated with xeric vegetation during the Holocene. Upward flow creates a drying front that propagates deeper into the profile with time and results in matric potentials similar to field-measured water potentials.

[39] Alternative conceptual models to upward flow may be appropriate for the High Plains site, where field-monitored water potentials can be simulated after 1 to 2 kyr of drying (Figure 14). Reduction in water flux from the Pleistocene ( $\sim 1.3$  mm/yr) to the Holocene ( $\sim 0.1$  mm/yr)

or zero flux for 8 kyr, followed by upward flux for 1 kyr, also reproduced the measured water potential and Cl profiles at this site. Therefore at this site a variety of alternative conceptual models are feasible. These alternative models are not appropriate for the other sites because long times are required to simulate the measured low water potentials.

[40] The conceptual model of xeric vegetation during the Holocene assumes that the root zone is fixed at a single time and remains at a fixed depth during the time required to accumulate Cl bulges ( $\sim 9$ – $16$  kyr). Fixing the root zone at a single time assumes that the transition from mesic to xeric vegetation occurred over a short timescale relative to the timescale for climate change. Assuming uniform rooting depth during the Holocene may not be appropriate because water potential and Cl profiles in some settings indicate that roots may extend to greater depths than represented in our models. In an ephemeral stream setting with extremely dense mesquite trees in the Eagle Flat Basin, low water potentials, with the typical curved exponential shape and very low Cl concentrations, suggest that deep-rooted mesquite trees can extract water from the subsurface and create low water potential profiles in shorter times than required to accumulate Cl (Figure 15). Roots of mesquite trees have been found to depths of  $\geq 6$  m in fissured sediments at the HB site [Scanlon, 1992]. Similar results were found by Walvoord [2002] in an area where juniper trees occur. Therefore, if the assumption of constant rooting depth over the Holocene fails, dense vegetation with much deeper roots may be able to create upward water potential gradients over much shorter time periods than required to accumulate Cl bulges.

#### 3.5.3.2. Hydraulic Parameterization

[41] Hydraulic parameterization was relatively simplistic for the simulations in this study. Most sites are represented by a homogenous sediment profile. The effect of varying sediment texture at the AD site was evaluated by replacing layer 1 with layer 3 material properties [Andraski and Jacobson, 2000]. Layer 3 has lower saturated water content (0.22) than layer 1 (0.29) and higher saturated hydraulic conductivity (3.2 m/d) by about an order of magnitude than layer 1 (0.4 m/d). Because of the linear effect of varying water content on simulated Cl concentrations, varying the porosity by  $\sim 25\%$  resulted in varying the simulated Cl concentrations by the same amount. Increasing the saturated hydraulic conductivity had little impact on simulated matric potentials because the drying process is controlled primarily by thermal vapor flux.

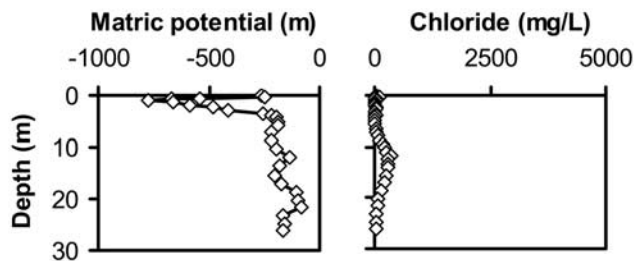


**Figure 15.** Water potential and Cl profiles in an area of dense mesquite trees in an ephemeral stream setting in the Eagle Flat Basin.

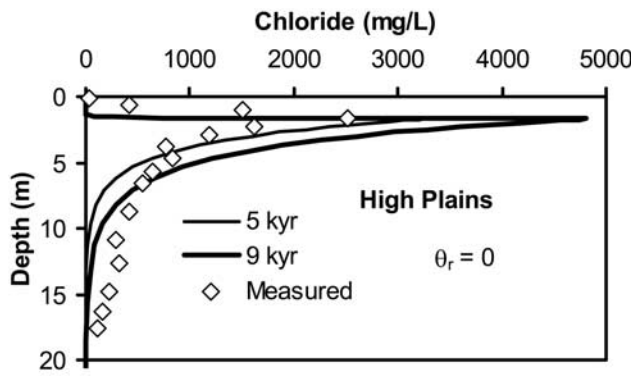


**Figure 16.** Simulated Cl profile for the HP site using a water retention function with zero residual water content. For comparison with nonzero residual water content ( $0.06 \text{ m}^3/\text{m}^3$ ), see Figure 9b.

[42] Although residual water content is treated as a fitting parameter in many retention functions, Ross *et al.* [1991] and Rossi and Nimmo [1994] indicated that it is more appropriate to set residual water content to zero at a finite matric potential ( $10^5 \text{ m}$ , equivalent to oven drying at  $105^\circ\text{C}$  at a room relative humidity of 50%). All simulations were rerun with zero residual water content, which resulted in water content at a matric potential of  $10^5 \text{ m}$  being reduced from 3–8% to 0–3% for the different materials. Simulated matric potentials were similar for zero and nonzero residual water contents. However, reducing residual water content reduced simulated water content and increased simulated Cl concentrations. The effect of reducing residual water content was greatest at the HP site because the original residual water content ( $0.06 \text{ m}^3/\text{m}^3$ ) was highest at this site and the resultant simulated peak Cl concentration increased by up to a factor of 2.6 (Figure 16).

[43] Simulated Cl profiles are also sensitive to varying other parameters in the water retention function, such as the van Genuchten n parameter. For example, varying n from 1.3 to 1.5 for the AD site had little impact on simulated matric potentials, but it decreased simulated water content and doubled simulated peak Cl concentration (Figure 17). These results demonstrate that simulated Cl profiles are very

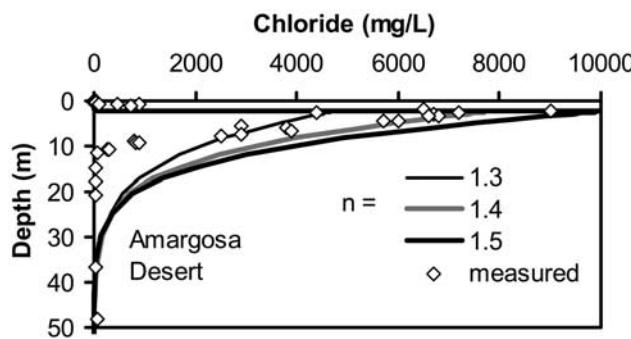


**Figure 17.** Effect of varying the water retention function (van Genuchten n parameter) on simulated Cl profiles at the AD site.

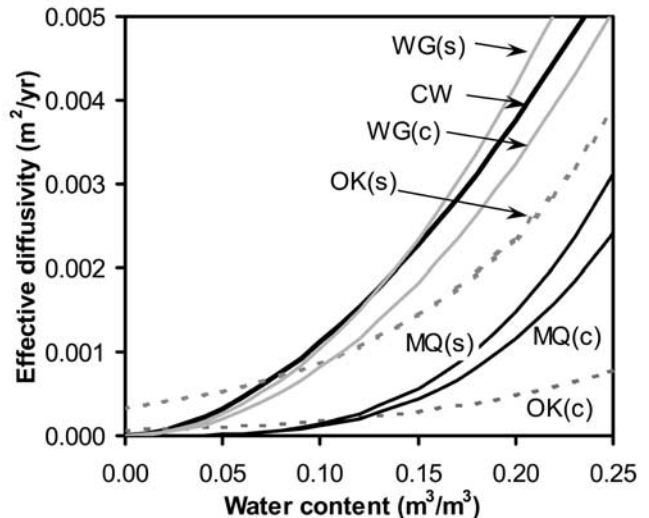


**Figure 18.** Effective diffusivity ( $D_e$ ) for Cl calculated using expressions from Millington and Quirk [1961] (MQ), Wilson and Gelhar [1974] (WG), and Olsen and Kemper [1968] (OK) for sand (s) and clay (c) and from Conca and Wright [1992] (CW; independent of sediment texture).

sensitive to water retention functions because of their dependence on simulated water content.

### 3.5.3.3. Cl Diffusion

[44] The main scenario evaluated in the modeling study was upward flow during the Holocene related to the root sink, which requires diffusion driven by concentration gradients to transport Cl below the root zone. Uncertainties related to Cl diffusion result primarily from uncertainties in the calculation of effective diffusivities ( $D_e$ ). Several expressions are described in the literature for calculating  $D_e$  (Figure 18). The Millington and Quirk [1961] equation ( $D_e = D_0 \theta^{10/3}/\phi$ ) was used to calculate  $D_e$  for most sites where  $D_0$  is Cl diffusivity in pure water ( $2.03 \times 10^{-9} \text{ m}^2/\text{s}$  [Cussler, 1984]) and  $\phi$  is porosity. The Conca and Wright [1992] equation ( $D_e = D_0 \theta^{1.76}$ ) was used for the AD site because it resulted in a better fit to the measured Cl concentrations. To evaluate the impact of different  $D_e$  values on simulated Cl profiles, Cl profiles for the AD and HB sites were simulated using both Millington and Quirk and Conca and Wright diffusion equations. The much higher  $D_e$  values estimated using the Conca and Wright equation result in more diffuse Cl profiles with lower peaks than those simulated using the Millington and Quirk equation (Figure 19). Recent studies by Schaefer *et al.* [1995] indicate that  $D_e$  values using a parallel liquid phase diffusion resistance model were up to two orders of magnitude greater than those based on the Millington and Quirk equation. The Schaefer model includes interparticle and intraparticle diffusion and indicates that diffusion becomes negligible at low water contents ( $\theta \sim 1$  to 2%), when only intraparticle diffusion occurs. Large uncertainties in  $D_e$  coefficients, particularly at low water contents, underscore the need for rigorous testing of existing models and possible development of new models.

### 3.6. Future Studies

[45] Results of the uncertainty analysis identify gaps in our knowledge and the need for additional research. The

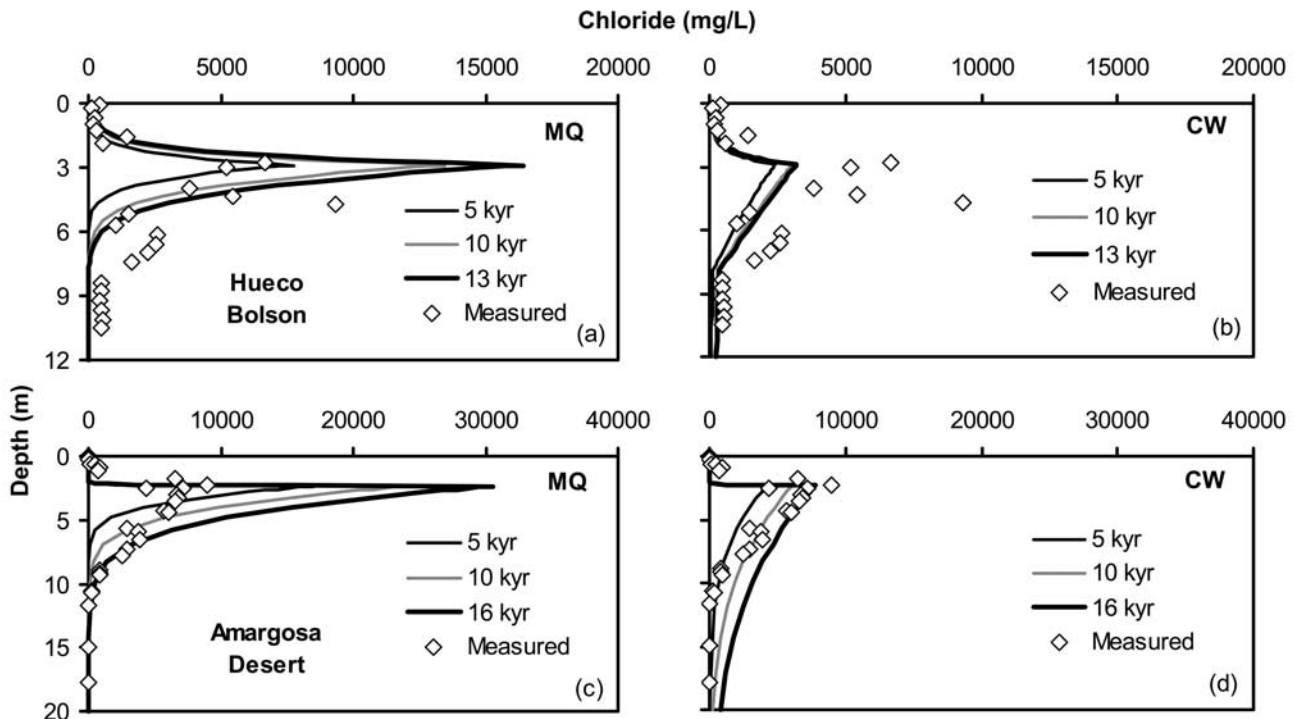


**Figure 19.** Effect of using Millington and Quirk [1961] (MQ) versus Conca and Wright [1992] (CW) effective diffusivities on simulated Cl profiles at the (a and b) Hueco Bolson and (c and d) Amargosa Desert sites. Measured Cl concentrations are shown for reference.

main sources of uncertainty evaluated in this study include (1) Cl input for the CMB estimated fluxes and ages, (2) osmotic component of water potential, (3) conceptual model, and (4) parameterization of the numerical models. Studies are currently being conducted by the U.S. Geological Survey to quantify spatial variability in Cl inputs at a number of sites in the southwestern United States (Izbicki, personal communication, 2000). However, it is much more difficult to determine whether Cl inputs have been temporally uniform over the timescales evaluated in this study. Uncertainties in the osmotic component of water potential should be evaluated by quantifying the osmotic potential and using codes that simulate osmotic potentials, such as that described by Nassar and Horton [1992]. The impact of the development of osmotic potentials on subsurface flow as Cl accumulated in the profile could be examined using these simulations.

[46] The modeling results from this study indicate that the formation of upward water potential gradients requires time periods at the same scale as those required to accumulate Cl. However, some profiles in areas of dense vegetation indicate that low water potentials and upward gradients can be developed over much shorter timescales than those required to accumulate Cl. Additional profiling should be conducted in similar settings to determine the prevalence of such conditions.

[47] The Philip and de Vries [1957] enhancement factor for thermal vapor conductivity is based on theory developed in the late 1950's. Because the enhancement factor based on experimental data from Cass *et al.* [1984] significantly increased thermal vapor fluxes at many of the sites considered in this study, the theoretical basis for the enhancement

factor should be reexamined, and additional laboratory studies should be conducted to evaluate the enhancement factor.

[48] Simulations in this study were relatively simplistic. The profiles at most sites were approximated using a single soil type. Future simulations should consider the effect of heterogeneity and layering on simulation results. The wide range of models available to estimate effective diffusivities ( $D_e$ ) for Cl transport and large uncertainties in  $D_e$ , particularly at low water contents, underscores the need for additional research on this topic. The importance of Cl diffusion at sites examined in this study can be tested further by measuring  $^{37}\text{Cl}/^{35}\text{Cl}$  ratios because the lighter  $^{35}\text{Cl}$  isotope should diffuse faster than the heavier  $^{37}\text{Cl}$  isotope [Walvoord, 2002]. Natural  $^{37}\text{Cl}/^{35}\text{Cl}$  ratios are fairly uniform ( $\pm 1$  per mil from standard mean ocean Cl [Eggenkamp, 1997]). If diffusive Cl transport is dominant beneath the Cl bulge, then  $^{37}\text{Cl}/^{35}\text{Cl}$  ratios should differ markedly from natural ratios. This approach was evaluated to a limited extent by Walvoord [2002] in Trans Pecos, Texas; however, the results were equivocal. Comparing the  $^{37}\text{Cl}/^{35}\text{Cl}$  ratios beneath the bulge at the EF site where the profile looks highly diffusive with those at the HB site, where the multipeaked Cl profile suggests low diffusion, would help in evaluating the importance of diffusion in these settings. These proposed studies should help to better constrain simulation results and provide more insight into flow and transport in thick desert vadose zones.

### 3.7. Implications

[49] The results of this analysis have important implications for water resources. Simulation results suggest that

deep water potential and Cl profiles are out of equilibrium with current climatic forcing. Water fluxes estimated from Cl profiles at depth represent paleofluxes during the Pleistocene (Table 1) and should not be used to estimate current water fluxes at depth. Simulation results indicate that current water fluxes at the base of the unsaturated zone differ in direction at some sites (HP and AD) and magnitude at all sites from CMB-calculated paleofluxes. Simulated water fluxes at the base of the unsaturated zone are almost three orders of magnitude less than that estimated by the CMB approach at the AD site. Therefore using the CMB approach to estimate recharge at this site would greatly overestimate water resource availability. In contrast, the similarity in CMB water fluxes and simulated water fluxes at the EF site is attributed to low water fluxes during Pleistocene and earlier times at this site, which were controlled by the fine-grained sediments.

[50] The results also have implications for waste disposal. Modeling results indicate that under present climatic conditions, the natural soil-plant system limits deep percolation of precipitation and contributes to upward water fluxes below the root zone. Thus waste cover systems that replicate the natural system could decrease the potential for precipitation to percolate downward and transport contaminants to underlying aquifers. However, changes in climate, disposal of liquids, and disturbances caused by construction of waste trenches and removal or replacement of native vegetation could negate positive waste isolation features of the natural system.

#### 4. Conclusions

[51] Unsaturated flow and transport were evaluated in thick desert vadose zones beneath native vegetation in the High Plains (HP), Texas; in the Hueco Bolson (HB) and Eagle Flat (EF) Basins in the Chihuahuan Desert, Texas; and in the Amargosa Desert (AD), Nevada. Upward water potential gradients indicate that current water fluxes in the shallow subsurface of interdrainage semiarid and arid regions are upward. Minimum water potentials measured near the surface were extremely low (down to  $-1000$  m), indicating very dry conditions. Long-term water potential monitoring (5–12 yr) shows that penetration of wetting fronts is restricted to the upper 0.3 to 3 m in response to seasonal fluctuations in precipitation. Low Cl concentrations beneath the Cl bulge at depths of  $\sim 10$  to 25 m represent higher water fluxes during the Pleistocene.

[52] The response of subsurface flow to paleoclimatic forcing varied among the sites as a function of sediment texture. The Cl inventory in fine-grained sediments at the EF site represents  $\sim 90$  kyr of accumulation in a 17.5-m-deep profile. High Cl concentrations ( $\sim 2600$  mg/L) at depth at this site represent low water fluxes (0.04 mm/yr) that persisted through the Pleistocene. In contrast, Cl inventories in coarse-grained sediments in the Chihuahuan and Amargosa Deserts represent  $\sim 12$  to 16 kyr of accumulation within the Cl bulge. Low Cl concentrations at depth (20–460 mg/L) represent higher water fluxes (8.4 to 0.2 mm/yr) during the Pleistocene. The site in the High Plains has fine-grained sediments; however, Cl concentrations are low at depth, which suggests high water fluxes during the Pleistocene (1.3 mm/yr).

[53] Numerical modeling of nonisothermal liquid and vapor flow indicates that development of upward water potential gradients requires thousands of years and that the water potential and Cl profiles at depth are out of equilibrium with current climatic forcing but reflect Pleistocene climate conditions. The simulations suggest that the drying front that was initiated during the Pleistocene/Holocene climate shift has propagated downward slowly with time. Downward Cl transport occurs by diffusion against upward water flux in the shallow subsurface. The shallower profiles (water table depth  $\sim 100$  m; HP and AD sites) have simulated upward total water flux throughout the unsaturated zone, whereas deeper profiles in the Chihuahuan Desert (water table depth  $\sim 200$  m) have a divergent total water flux pattern with upward water fluxes in the upper 40 to 115 m depth and downward water fluxes below this zone. The relative importance of liquid and vapor flux varies among the sites as a result of variations in climate and sediment textures. Vapor flux is negligible at the HP site, where the sediments are fine grained and climate is wetter, whereas vapor fluxes are higher in the AD profile and in the upper 8 m of the HB profile, where the sediments are coarse grained and dry. Vapor fluxes at these sites are dominated by thermal vapor fluxes.

[54] Integration of soil-physics monitoring and environmental-tracer profiles with numerical modeling provided a comprehensive understanding of subsurface flow processes under current and past climatic conditions. The results of this study have important implications for water resources and indicate that current recharge in interdrainage desert regions is negligible. These results also suggest that soil-plant-atmosphere interactions should be considered in the design and evaluation of waste-disposal sites in interdrainage desert settings.

[55] **Acknowledgments.** This project was funded in part by the U.S. Department of Energy. The senior author benefited from many helpful discussions with Michelle Walvoord. We gratefully acknowledge reviews provided by Mitchell Plummer, David Stonestrom, and two anonymous reviewers.

#### References

- Andraski, B. J., Properties and variability of soil and trench fill at an arid waste-burial site, *Soil Sci. Soc. Am. J.*, 60, 54–66, 1996.
- Andraski, B. J., Soil-water movement under natural-site and waste-site conditions: A multi-year field study in the Mojave Desert, Nevada, *Water Resour. Res.*, 33, 1901–1916, 1997.
- Andraski, B. J., and E. A. Jacobson, Testing a full-range soil-water retention function in modeling water potential and temperature, *Water Resour. Res.*, 36, 3081–3090, 2000.
- Andraski, B. J., and D. E. Prudic, Soil, plant, and structural considerations for surface barriers in an arid environment—Application of results from studies in the Mojave Desert, in *Barriers for Environmental Management, Summary of a Workshop*, pp. D50–D60, Natl. Acad. Press, Washington, D. C., 1997.
- Andraski, B. J., and B. R. Scanlon, Thermocouple psychrometry, in *Methods of Soil Analysis*, part 4, *Physical Methods*, edited by J.H. Dane and G. C. Topp, pp. 609–642, Soil Sci. Soc. of Am., Madison, Wis., 2002.
- Benson, L. V., D. R. Currey, R. I. Dorn, K. R. Lajoie, C. G. Oviatt, S. W. Robinson, G. I. Smith, and S. Stine, Chronology of expansion and contraction of four Great Basin lake systems during the past 35,000 years, *Palaeogeogr. Palaeoclimatol. Palaeoecol.*, 78, 241–286, 1990.
- Campbell, G. S., *Soil Physics With BASIC: Transport Models for Soil-Plant Systems*, Elsevier Sci., New York, 1985.
- Cass, A., G. S. Campbell, and T. L. Jones, Enhancement of thermal water vapor diffusion in soil, *Soil Sci. Soc. Am. J.*, 48, 25–32, 1984.
- Chung, S. O., and R. Horton, Soil heat and water flow with a partial surface mulch, *Water Resour. Res.*, 23, 2175–2186, 1987.

- Conca, J. L., and J. V. Wright, Diffusion and flow in gravel, soil, and whole rock, *Appl. Hydrogeol.*, 1, 5–24, 1992.
- Cussler, E. L., *Diffusion: Mass Transfer in Fluid Systems*, Cambridge Univ. Press, New York, 1984.
- Davis, S. N., D. O. Whittemore, and J. Fabryka-Martin, Uses of chloride/bromide ratios in studies of potable water, *Ground Water*, 36, 338–350, 1998.
- Eggenkamp, H. G. M., *The Geochemistry of Chlorine Isotopes*, Utrecht Univ., Utrecht, Netherlands, 1997.
- Fayer, M. J., UNSAT-H version 3.0: Unsaturated soil water and heat flow model, theory, user manual, and examples, *Rep. 13249*, Pac. Northwest Natl. Lab., Richland, Wash., 2000.
- Fischer, J. M., Sediment properties and water movement through shallow unsaturated alluvium at an arid site for disposal of low-level radioactive waste near Beatty, Nye County, Nevada, *U.S. Geol. Surv. Water Resour. Invest. Rep.*, 92-4032, 48 pp., 1992.
- Fouty, S. C., Cl mass balance as a method for determining long-term groundwater recharge rates and geomorphic-surface stability in arid and semi-arid regions: Whisky Flat and Beatty, Nevada, M.Sc. Univ. of Ariz., Tucson, 1989.
- Henry, C. D., and J. K. Gluck, A preliminary assessment of the geologic setting, hydrology, and geochemistry of the Hueco Tanks Geothermal Area, Texas and New Mexico, *Geol. Circ. Univ. Tex. Austin Bur. Econ. Geol.*, 81-1, 48 pp., 1981.
- Holliday, V. T., Stratigraphy and paleoenvironments of late Quaternary valley fills on the Southern High Plains, *Mem. Geol Soc. Am.*, 186, 136 pp., 1995.
- Izbicki, J. A., et al., Water movement through a thick unsaturated zone underlying an intermittent stream in the western Mojave Desert, southern California, *J. Hydrol.*, 238, 194–217, 2000.
- Jury, W. A., W. R. Gardner, and W. H. Gardner, *Soil Physics*, John Wiley, New York, 1991.
- Leij, F. J., W. J. Alves, M. T. van Genuchten, and J. R. Williams, The UNSODA unsaturated soil hydraulic database, user's manual, version 1.0.EPA/600/R-96/095, Natl. Risk Manage. Lab., Off. of Res. and Develop., U.S. Environ. Prot. Agency, Cincinnati, Ohio, 1996.
- Millington, R. J., and J. P. Quirk, Permeability of porous solids, *Trans. Faraday Soc.*, 57, 1200–1207, 1961.
- Morrison, R. B., Quaternary stratigraphic, hydrologic, and climatic history of the Great Basin, with emphasis on Lakes Lahontan, Bonneville and Tecopa, in *Quaternary Nonglacial Geology: Conterminous U.S.*, vol. K-2, *The Geology of North America*, edited by R. B. Morrison, pp. 283–320, Geol. Soc. of Am., Boulder, Colo., 1991.
- Mualem, Y., A new model for predicting the hydraulic conductivity of unsaturated porous media, *Water Resour. Res.*, 12(3), 513–521, 1976.
- Musgrove, M., J. L. Banner, L. E. Mack, D. M. Combs, E. W. James, H. Cheng, and R. L. Edwards, Geochronology of late Pleistocene to Holocene speleothems from central Texas: Implications for regional paleoclimate, *Geol. Soc. Am. Bull.*, 113, 1532–1543, 2001.
- Nassar, I. N., and R. Horton, Simultaneous transfer of heat, water, and solute in porous media; 1, Theoretical development, *Soil Sci. Soc. Am. J.*, 56, 1350–1356, 1992.
- Olsen, S. R., and W. D. Kemper, Movement of nutrients to plant roots, *Adv. Agron.*, 20, 91–151, 1968.
- Philip, J. R., and D. A. de Vries, Moisture movement in porous materials under temperature gradients, *Eos Trans. AGU*, 38, 222–232, 1957.
- Phillips, F. M., Environmental tracers for water movement in desert soils of the American Southwest, *Soil Sci. Soc. Am. J.*, 58, 14–24, 1994.
- Prudic, D. E., Estimates of percolation rates and ages of water in unsaturated sediments at two Mojave Desert sites, California-Nevada, *U.S. Geol. Surv. Water Resour. Invest. Rep.*, 94-4160, 19 pp., 1994.
- Prych, E. A., Using chloride and chlorine-36 as soil-water tracers to estimate deep percolation at selected locations on the U.S. Department of Energy Hanford Site, Washington, *U.S. Geol. Surv. Water Supply Pap.*, 2481, 67 pp., 1998.
- Quade, J., Late Quaternary environmental changes in the upper Las Vegas Valley, Nevada, *Quat. Res.*, 26, 340–357, 1986.
- Reith, C. C., and B. M. Thompson, *Deserts as Dumps? The Disposal of Hazardous Materials in Arid Ecosystems*, Univ. of N.M. Press, Albuquerque, 1992.
- Ross, B., A conceptual model of deep unsaturated zones with negligible recharge, *Water Resour. Res.*, 20, 1627–1629, 1984.
- Ross, P. J., J. Williams, and K. L. Bristow, Equation for extending water-retention curves to dryness, *Soil Sci. Soc. Am. J.*, 55, 923–927, 1991.
- Rossi, C., and J. R. Nimmo, Modeling of soil water retention from saturation to oven dryness, *Water Resour. Res.*, 30, 701–708, 1994.
- Scanlon, B. R., Evaluation of moisture flux from Cl data in desert soils, *J. Hydrol.*, 128, 137–156, 1991.
- Scanlon, B. R., Moisture and solute flux along preferred pathways characterized by fissured sediments in desert soils, *J. Contam. Hydrol.*, 10, 19–46, 1992.
- Scanlon, B. R., Water and heat fluxes in desert soils: 1. Field studies, *Water Resour. Res.*, 30, 709–719, 1994.
- Scanlon, B. R., Uncertainties in estimating water fluxes and residence times using environmental tracers in an arid unsaturated zone, *Water Resour. Res.*, 36, 395–409, 2000.
- Scanlon, B. R., and R. S. Goldsmith, Field study of spatial variability in unsaturated flow beneath and adjacent to playas, *Water Resour. Res.*, 33, 2239–2252, 1997.
- Scanlon, B. R., and P. C. D. Milly, Water and heat fluxes in desert soils: 2. Numerical simulations, *Water Resour. Res.*, 30, 721–733, 1994.
- Scanlon, B. R., F. P. Wang, and B. C. Richter, Field studies and numerical modeling of unsaturated flow in the Chihuahuan Desert, Texas, *Rep. Invest. Univ. Tex. Austin Bur. Econ. Geol.*, 199, 56 pp., 1991.
- Scanlon, B. R., R. P. Langford, and R. S. Goldsmith, Relationship between geomorphic settings and unsaturated flow in an arid setting, *Water Resour. Res.*, 35, 983–999, 1999.
- Scanlon, B. R., R. S. Goldsmith, and R. P. Langford, Relationship between arid geomorphic settings and unsaturated zone flow: case study, Chihuahuan Desert, Texas, *Rep. Invest. Univ. Tex. Austin Bur. Econ. Geol.*, 261, 133 pp., 2000.
- Scanlon, B. R., B. J. Andraski, and J. Bilskie, Miscellaneous methods for measuring matric or water potential, in *Methods of Soil Analysis*, part 4, *Physical Methods*, edited by J. H. Dane and G. C. Topp, pp. 643–670, Soil Sci. Soc. of Am., Madison, Wis., 2002.
- Schaefer, C. E., R. R. Arands, H. A. van der Sloot, and D. S. Kosson, Prediction and experimental validation of liquid-phase diffusion resistance in unsaturated soils, *J. Contam. Hydrol.*, 20, 145–166, 1995.
- Simunek, J., M. Sejna, and M. T. van Genuchten, The HYDRUS-1D software package for simulating the one-dimensional movement of water, heat, and multiple solutes in variably-saturated media, version 2.0, *IGWMC - TPS - 70*, 202 pp., Int. Groundwater Model. Cent., Colo. Sch. of Mines, Golden, Colo., 1998.
- Spaulding, W. G., Vegetational and climatic development of the Mojave Desert: The Last Glacial Maximum to the present, in *Packrat Middens: The Last 40,000 Years of Biotic Change*, edited by J. L. Betancourt, T. R. van Devender, and P. S. Martin, pp. 166–199, Univ. of Ariz. Press, Tucson, 1990.
- Tyler, S. W., J. B. Chapman, S. H. Conrad, D. P. Hammermeister, D. O. Blout, J. J. Miller, M. J. Sully, and J. M. Ginanni, Soil-water flux in the southern Great Basin, United States: Temporal and spatial variations over the last 120,000 years, *Water Resour. Res.*, 32, 1481–1499, 1996.
- van Devender, T. R., Late Quaternary vegetation and climate of the Chihuahuan Desert, United States and Mexico, in *Packrat Middens: The Last 40000 Years of Biotic Change*, edited by J. L. Betancourt, T. R. van Devender, and P. S. Martin, pp. 104–133, Univ. of Ariz. Press, Tucson, 1990.
- van Genuchten, M. T., A closed-form equation for predicting the hydraulic conductivity of unsaturated soils, *Soil Sci. Soc. Am. J.*, 44, 892–898, 1980.
- Walvoord, M. A., A unifying conceptual model to describe water, vapor, and solute transport in deep arid vadose zones, Ph.D. thesis, N.M. Inst. of Mining and Technol., Socorro, 2002.
- Walvoord, M. A., M. A. Plummer, F. M. Phillips, and A. V. Wolfsberg, Deep system hydrodynamics: 1. Equilibrium states and response times in thick desert vadose zones, *Water Resour. Res.*, 38(12), 1308, doi:10.1029/2001WR000824, 2002.
- Wilkins, D. E., and D. R. Currey, Timing and extent of late Quaternary paleolakes in the Trans-Pecos closed basin, west Texas and south-central New Mexico, *Quat. Res.*, 47, 306–315, 1997.
- Wilson, J. L., and L. W. Gelhar, Dispersive mixing in a partially saturated porous medium, 191 pp., Dep. of Civ. Eng., Mass. Inst. Technol., Cambridge, 1974.
- K. Keese, R. C. Reedy, and B. R. Scanlon, Bureau of Economic Geology, Jackson School of Geosciences, University of Texas at Austin, 10100 Burnet Rd., Austin, TX 78758, USA. (bridget.scanlon@beg.utexas.edu; bob.reedy@beg.utexas.edu)
- J. Simunek, George E. Brown Jr., Salinity Laboratory, 450 W. Big Springs Road, Riverside, CA 92507, USA. (jsimunek@ussl.ars.usda.gov)
- B. J. Andraski, U.S. Geological Survey, 333 W. Nye Lane, Carson City, NV 89706, USA. (andraski@usgs.gov)

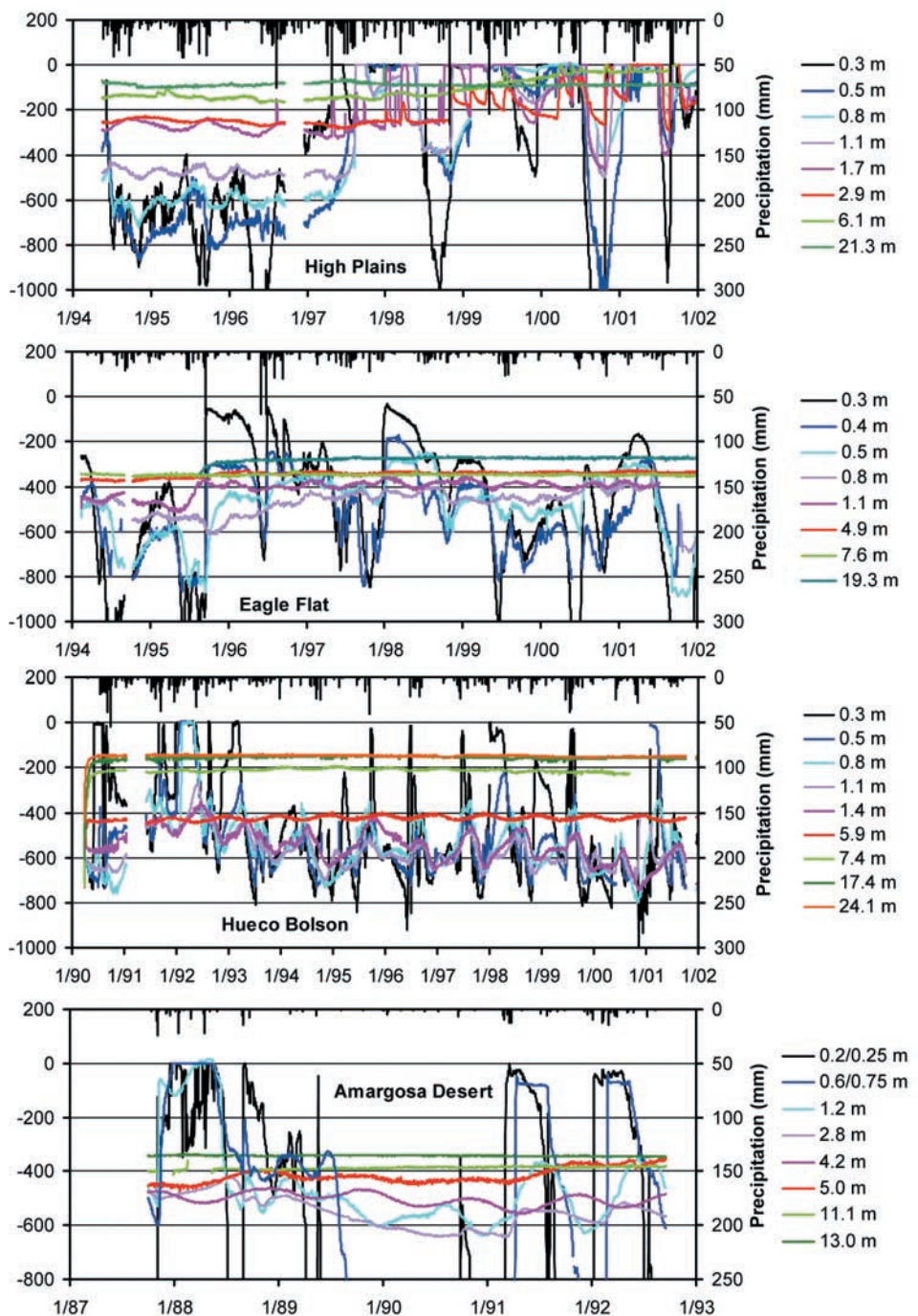


**Figure 5.** Temporal variability in water potential monitored in situ at various depths at each site. Daily precipitation is also shown.